Pflugers Arch - Eur J Physiol (2016) 468:1223–1240
DOI 10.1007/s00424-016-1816-7



# Human CNNM2 is not a $Mg^{2+}$ transporter per se

**Gerhard Sponder[1] · Lucia Mastrototaro[1] · Katharina Kurth[1,5] · Lucia Merolle[2,6] · Zheng Zhang[3] · Nasrin Abdulhanan[1] · Alina Smorodchenko[1,7] · Katharina Wolf[1] · Andrea Fleig[3] · Reinhold Penner[3] · Stefano Iotti[2] · Jörg R. Aschenbach[1] · Jürgen Vormann[4] · Martin Kolisek[1]**

Received: 19 December 2015 / Revised: 15 March 2016 / Accepted: 23 March 2016 / Published online: 11 April 2016


**Abstract** CNNM2 is associated with the regulation of serum Mg concentration, and when mutated, with severe familial hypomagnesemia. The function and cellular localization of CNNM2 and its isomorphs (Iso) remain controversial. The objective of this work was to examine the following: (1) the transcription-responsiveness of *CNNM2* to Mg starvation, (2) the cellular localization of Iso1 and Iso2, (3) the ability of Iso1 and Iso2 to transport $Mg^{2+}$, and (4) the complex-forming ability and spectra of potential interactors of Iso1 and Iso2. The five main findings are as follows. (1) Mg-starvation induces *CNNM2* overexpression that is markedly higher in JVM-13 cells (lymphoblasts) compared with Jurkat cells (T-lymphocytes). (2) Iso1 and Iso2 localize throughout various subcellular compartments in transgenic HEK293 cells overexpressing Iso1 or Iso2. (3) Iso1 and Iso2 do not transport $Mg^{2+}$ in an electrogenic or electroneutral mode in transgenic HEK293 cells overexpressing Iso1 or Iso2. (4) Both Iso1 and Iso2 form complexes of a higher molecular order. (5) The spectrum of potential interactors of Iso1 is ten times smaller than that of Iso2. We conclude that sensitivity of *CNNM2* expression to extracellular $Mg^{2+}$ depletion depends on cell type. Iso1 and Iso2 exhibit a dispersed pattern of cellular distribution; thus, they are not exclusively integral to the cytoplasmic membrane. Iso1 and Iso2 are not $Mg^{2+}$ transporters per se. Both isomorphs form protein complexes, and divergent spectra of potential interactors of Iso1 and Iso2 indicate that each isomorph has a distinctive function. CNNM2 is therefore the first ever identified $Mg^{2+}$ homeostatic factor without being a $Mg^{2+}$ transporter per se.

**Keywords** Magnesium · Homeostasis · Patch clamp · Mag-fura 2 · Protein interactions · Mitochondria

Gerhard Sponder, Lucia Mastrototaro, Katharina Kurth, Lucia Merolle and Zheng Zhang contributed equally to this work.

**Electronic supplementary material** The online version of this article (doi:10.1007/s00424-016-1816-7) contains supplementary material, which is available to authorized users.

✉ Martin Kolisek
martink@zedat.fu-berlin.de

[1] Institute of Veterinary-Physiology, Free University of Berlin, Oertzenweg 19b, 14163 Berlin, Germany

[2] Department of Pharmacy and Biotechnology, University of Bologna, Via Massarenti 9, Bologna, Italy

[3] The Queen's Medical Center, Center for Biomedical Research, 1356 Lusitana Street, UH Tower 8, Honolulu, HI, USA

[4] Institute for Prevention and Nutrition (IPEV), Adalperostrasse 37, Munich, Ismaning, Germany

[5] Present address: Landesuntersuchungsanstalt Sachsen, Jägerstraße 8/10, Dresden, Germany

[6] Present address: Elettra—Sincrotrone Trieste S.C.p.A., Strada Statale 14 AREA Science Park, Basovizza, Italy

[7] Present address: Institute of Vegetative Anatomy, Charité - Universitätsmedizin Berlin, Campus Charité Mitte, Philippstrasse 12, Berlin, Germany

## Introduction

The importance of magnesium (Mg) for a plethora of core cellular processes has been described in numerous monographs. The free intracellular $Mg^{2+}$ concentration ($[Mg^{2+}]_i$) of mammalian cells is held between a relatively narrow range of approximately 0.2 and 1 mM (representing approximately 5 % of the total Mg of the cell) by $Mg^{2+}$-regulatory mechanisms ($Mg^{2+}$-homeostatic factors, $Mg^{2+}$ transporters) [28]. Apart from the major cellular $Mg^{2+}$ influx pathway constituted by transient receptor potential melastatin channel kinases TRPM6 and TRPM7 (transient receptor potential cation channel subfamily M member 6 and 7; UniProt ID Q9BX84 and Q96QT4) [25], mitochondrial $Mg^{2+}$ channel Mrs2p (magnesium transporter Mrs2; Q9HD23) [16], ubiquitous $Na^+/Mg^{2+}$ exchanger solute carrier 41 member A1 (SLC41A1; Q8IVJ1) [9, 18], and $Mg^{2+}$ transporter magnesium transporter protein 1 (MagT1; Q9H0U3) [46], several other genes have been found to encode for proteins potentially transporting $Mg^{2+}$ or regulating intracellular $Mg^{2+}$ homeostasis (IMH), including CNNM2 (cyclin and CBS-domain divalent metal cation transport mediator 2, Q9H8M5) [10, 31].

*CNNM2* has been mapped to chromosome 10q24.32 (http://www.genecards.org/cgi-bin/carddisp.pl?gene=CNNM2). It is ubiquitously expressed with the highest levels having been measured in kidney and brain [10, 31] and encodes a protein with a molecular weight of approximately 97 kDa (www.phosphosite.org). Three distinctive splice variants (sp.v.) of *CNNM2* have been identified. Previously, we have demonstrated a functional disparity between isomorph 1 (Iso1) and 2 (Iso2) in complementation tests in *Salmonella enterica sv. Typhimurium* (strain MM281) [40]. Whereas Iso1 is clearly capable of transporting $Mg^{2+}$, Iso2 is not [40]. Goytain and Quamme have demonstrated that Iso1 transiently overexpressed in *Xenopus* oocytes conducts the electrogenic transport of $Mg^{2+}$ (and also $Co^{2+}$, $Mn^{2+}$, $Sr^{2+}$, $Ba^{2+}$, $Cu^{2+}$, and $Fe^{2+}$) [10, 31]. The shortest Iso, namely Iso3, has not been experimentally studied as yet, perhaps because of the lack of CBS (the dimerization/regulatory domains) and the C-terminal CorC-HlyC domain, which are otherwise present in Iso1 and Iso2 [40]. The only difference between Iso1 and Iso2 is the region between amino acids 722 and 743 of Iso1, which is missing in Iso2 [40]. The latter region might therefore be important either for $Mg^{2+}$ binding, $Mg^{2+}$ binding-site assembly, or the determination of the operational mode of Iso1 [40].

Human CNNM2 (also known as ACDP2) was originally described as being a nuclear protein in HeLa cells [45]. De Baaij and colleagues have examined the pathways of CNNM2 maturation and posttranslational modification and proposed that an endoplasmic reticulum (ER) signal peptidase mediates the cleavage of a large N-terminal signal peptide of about 64 amino acids [7]. According to this model, the mature protein possesses three transmembrane helices (TH) with an "N-terminus outside, C-terminus inside" configuration [7]. Furthermore, they have shown that the glycosylation of Asn-112 contributes to CNNM2 stability in the plasma membrane [7]. Although the experimental evidence supports that CNNM2 is a protein integral primarily to the cytoplasmic membrane [7], the possibility that it might also be localized to intracellular membranous structures has never clearly been ruled out.

The function of CNNM2 has not as yet been described satisfactorily. Goytain and Quamme [10], our group [40], and Stuiver and coworkers [41] have demonstrated its involvement in the regulation of IMH; however, the CNNM2-related $Mg^{2+}$ transport seen in a heterologous expression system [10, 31, 40] has not been confirmed in a homologous expression system [41]. The possibility that CNNM2 transports $Mg^{2+}$ in an electroneutral mode has not been excluded.

Nevertheless, the strongest evidence for an involvement of CNNM2 in IMH, and perhaps also in systemic Mg homeostasis, comes from the work of Stuiver and coworkers who have associated a mutation in CNNM2 with dominant hypomagnesemia in Man [41]. Furthermore, common variants of *CNNM2* have been associated with the regulation of serum Mg concentrations in a genome-wide association study (GWAS) [23]. Based on GWAS, a possible link between CNNM2 and the susceptibility to ischemic stroke and coronary artery disease has also been established [43]. The identification of a schizophrenia risk variant rs7914558 is noteworthy, as is its possible impact on neural systems relevant to social cognition through the gray matter volumetric vulnerability of the orbital regions in the inferior frontal *gyri* [29, 34]. Moreover, mutations directly associated with impaired brain development and seizures in patients with hypomagnesemia have been identified [1].

Therefore, based on the circumstantial evidence that links CNNM2 to impaired IMH, the aim of the present study has been to examine the responsiveness of CNNM2 expression to extracellular $Mg^{2+}$ depletion, to study the cellular topography of Iso1 and Iso2, to examine the ability of CNNM2 (and its isomorphs, Iso1 and Iso2) to transport $Mg^{2+}$, and to characterize the complex-forming ability and possible molecular interactors of Iso1 and Iso2, respectively.

## Material and methods

### Cell cultures

The following cell types were used:

Jurkat (human T cell leukemia) and JVM-13 (human chronic B cell leukemia) cells were purchased from the German Collection of Microorganisms and Cell Cultures (DSMZ).

HEK293(tet)↑(Strep-HA-CNNM2sp.v.1): stable tetracycline-(tet)-inducible HEK293 cells overexpressing N-terminal Strep-HA-tagged Iso1; referred to as Iso1 cells.

HEK293(tet)↑(Strep-HA-CNNM2sp.v.2): stable tet-inducible HEK293 cells overexpressing N-terminal Strep-HA-tagged Iso2; referred to as Iso2 cells.

Iso1 and Iso2 cell lines were derived from Flp-In™ T-Rex-HEK293 cells (Invitrogen) and stably transfected with p*N-TGSH/CNNM2 sp.v.1* (NCBI: NM_017649.4) or *sp.v.2* (NCBI: NM_199076.2) (Dualsystems Biotech AG).

HEK293(tet)↑(CNNM2sp.v.1-Strep-His): transient tet-inducible HEK293 cells over-expressing CNNM2 Iso1 with a C-terminal Strep-Histag; referred to as Iso1-Strep cells.

HEK293(tet)↑(CNNM2sp.v.2-Strep-His): transient tet-inducible HEK293 cells overexpressing CNNM2 Iso2 with a C-terminal Strep-His-tag; referred to as Iso2-Strep cells.

Transient Iso1-Strep and Iso2-Strep cells were constructed by using the p*cDNA5/TO* vector system (Life Technologies), which allows for tet-inducible expression.

### Cell culture media

Jurkat and JVM-13 cells: Cells were cultured in RPMI1640 (PAN-Biotech) supplemented with 4.5 g/L glucose, 10 % fetal bovine serum (FBS; PAN-Biotech), 1 % PenStrep (PAN-Biotech), and Normocin™ (100 μg/mL, Cayla/InvivoGen) at 37 °C and under a 5 % $CO_2$ atmosphere according to DSMZ guidelines.

Iso1 and Iso2 cells: Cells were grown in complete DMEM (PAN-Biotech) supplemented with 4.5 g/L glucose, 10 % FBS (PAN-Biotech), and Ultra-glutamine. Blasticidin (15 μg/mL, Cayla/InvivoGen) and hygromycin (100 μg/mL, Cayla/InvivoGen) were provided. Cells were cultured to approximately 75–80 % confluency under a 5 % $CO_2$ atmosphere at 37 °C. Overexpression of Iso1 and Iso2 was induced by addition of tet (1 μg/mL) 24 h prior to cell harvest.

Iso1-Strep and Iso2-Strep cells: Cells were grown in complete DMEM (PAN-Biotech) supplemented with 4.5 g/L glucose, 10 % FBS (PAN-Biotech), and Ultra-glutamine. Blasticidin (15 μg/mL) was provided. HEK293-derived cell lines were cultured to approximately 75–80 % confluency under a 5 % $CO_2$ atmosphere at 37 °C. Overexpression of Iso1 and Iso2 was induced by addition of tet (1 μg/mL) 24 h prior to cell harvest or cell fixation.

### Cloning of CNNM2 Iso1 and 2 with a C-terminal Strep-His-tag

The coding sequence of *CNNM2 sp.v.2* was PCR-amplified from HEK293 cDNA with the forward primer CNNfw: 5′-ATGGTACCATGATTGGCTGTGGCGCTTGTGAACC-3′ (*Kpn*I restriction site underlined) and the reverse primer CNNrev: 5′-ATCTCGAGCTAGATGGCGCC TTCGTTGTGCAGG-3′ (*Xho*I restriction site underlined). The sequence was cloned via the abovementioned restriction sites into p*cDNA5/TO* (Thermo Fisher Scientific), and correctness was controlled by bidirectional sequencing. The last 749 bp of the cloned sequence was then cut out by using the restriction site *Msc*I and *Xho*I and replaced by sequences corresponding to *CNNM2 sp.v.1* or *sp.v.1* with a 3′ 6xHis-Strep-tag. The replacement sequences including the coding sequence for the 6xHis-Strep-tag were produced by gene synthesis.

### $Mg^{2+}$ starvation

Cells were grown to a density of about $1–2 \times 10^6$ cells/mL. Approximately $0.8 \times 10^6$ cells/mL were seeded into $Mg^{2+}$-free Hank's Balanced Salt Solution (HBSS—medium complemented with dialyzed nominally $Mg^{2+}$-free FBS (10 %; PAN Biotech) and PenStrep (1 %)). Samples used for RNA isolation were collected at the following time points: 0, 0.5, 1, 1.5, 2, 2.5, 3, 5, 8, 12, 24, and 48 h.

### RNA isolation and cDNA synthesis

Total RNA was isolated with the NucleoSpin RNA II kit (Macherey-Nagel) according to manufacturer's protocol. The integrity, purity, and amount of RNA were determined by using an Agilent 2100 Bioanalyzer (Agilent Technologies) and the Nanodrop ND-1000 (Peqlab Biotechnologie). RNA integrity number exceeded 9 in all samples. Possible genomic DNA contamination of each sample was tested by PCR when using RNA eluate instead of cDNA as a template. Synthesis of cDNA was performed with an iScript cDNA-synthesis kit (Bio-Rad) according to the manufacturer's protocol.

### qRT-PCR and data analysis

The gene-specific primer pairs and their sequences were as described in Kolisek et al. [19]. Appropriate primer-annealing conditions were assessed for each respective primer pair by temperature gradient PCR (tg-PCR; with the cycler Primus 96; Peqlab Biotechnologie). The best primer-annealing conditions and the specificity were estimated by agarose electroseparation. SYBR-green-based quantitative real-time PCR (qRT-PCR) was performed with an iCycler iQ (Bio-Rad) in a two-step protocol (35 cycles: 30 s at 95 °C, 2 min at 58 °C). *Tuba1b* served as a reference gene. The M value (gene stability) determined by software geNorm (qbase+, biogazelle) for *Tuba1b* was 0.172 in Jurkat cells and 0.417 in JVM-13 cells and, therefore, in both cases, below the maximum acceptable value of 0.5. The expression activities of the Mg-responsive (magnesiotropic) genes (*MRG*s) were determined as the $C_T$ difference (GED) in gene expression according to the formula of Schefe et al. [37] (Fig. 1). The threshold of significance of gene expression changes was set to GED = −1 and +1. The normalized gene expression values of the Jurkat and JVM-13 samples were calculated against the

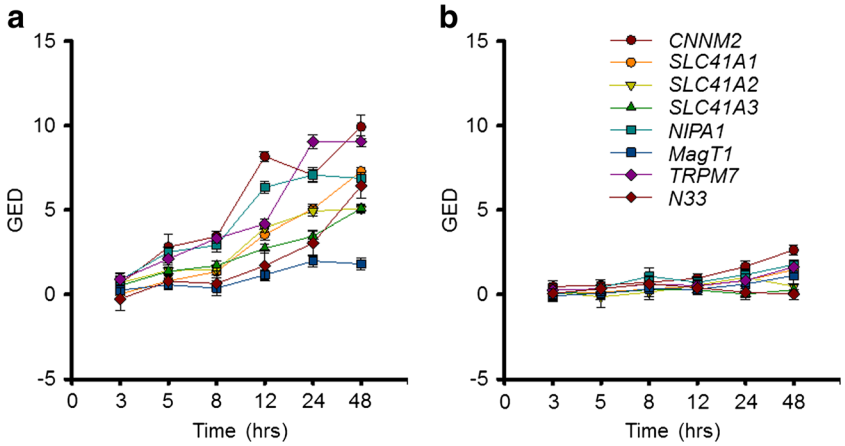


**Fig. 1** *MRGs* expression's $C_T$ difference monitored at indicated time points in **a** JVM-13 and **b** Jurkat cells incubated in nominally $Mg^{2+}$-free medium. Legend in panel **b** applies also to panel **a**. Data are presented as means ± SE (*N/n* = 3/9). Tested *MRGs*: *CNNM2*, cyclin and CBS-domain divalent metal cation transport mediator 2; *MagT1*, magnesium transporter protein 1; *N33*, tumor suppressor candidate 3; *NIPA1*, protein non imprinted in Prader-Willi/Angelman syndrome 1; *SLC41A1/A2/A3*, solute carrier family 41 member A1 or A2 or A3; *TRPM7*, transient receptor potential cation channel subfamily M member 7. Abbreviations: *GED*, gene expression's $C_T$ difference; *hrs*, hours; *MRGs*, magnesiotropic genes

values obtained from samples collected at time 0 h for every respective experimental series. Data acquisition, processing, and evaluation are coherent with MIQE guidelines [5].

### Confocal microscopy

Cells were fixed as described by Kolisek at al. [17]. After the cells had been washed with phosphate-buffered saline (PBS), a blocking step with normal goat serum (NGS, Abcam) (10 % in PBS) was performed. Then, the cells were incubated for 1 h with the primary antibody (Ab) diluted in 1 % NGS. For detection of N-terminally or C-terminally Strep-tagged Iso1 and Iso2, a primary anti-Strep Ab (diluted 1:500; Qiagen) was used. Native (background) and transgenic Iso1 and Iso2 were also detected with rabbit polyclonal Ab directed against the native CNNM2 epitope (AA575–AA625; diluted 1:1000; Abgent). Cells were washed thrice in PBS and incubated with the secondary Ab diluted 1:500 in 1 % NGS; goat anti-mouse Ab conjugated with Alexa-Green (488 nm, Invitrogen) was used for the Strep-Ab and goat anti-rabbit Ab conjugated with Alexa-Red (561–594 nm, Invitrogen) for the CNNM2-Ab.

For the colocalization study, double-stain immunofluorescence was performed. Cells were incubated simultaneously with primary Ab, mouse anti-Strep, and rabbit anti-mitochondrial cytochrome c oxidase IV (COXIV; Cell Signaling Technology) Ab and subsequently with the secondary Ab, goat anti-mouse (green), and goat anti-rabbit (red), respectively. Where indicated, mitochondria were stained with MitoTracker Green FM (Thermo Fisher Scientific).

Processed samples were mounted. Where indicated, Fluoroshield-4′,6-diamino-2-phenylindol (DAPI; Abcam) was used to visualize nuclei. Confocal images were taken with a confocal laser scanning microscope LSM 510 META (Carl Zeiss). ImageJ software (http://rsb.info.nih.gov/ij/) or Carl Zeiss AIM LSM Software 3.2 SP2 were used for image merging.

### Whole cell mode patch clamp of Iso1 and Iso2 HEK293 cells

Experiments were performed at room temperature. Data were acquired with Pulse software (EPC-9 amplifier; HEKA) at settings as described in Schmitz et al. [38]. Coverslip-grown −tet and +tet Iso1 and Iso2 or TRPM7 (tet induction 15 h) HEK293 cells were kept in a Ringer solution composed (in mM) of NaCl 140, KCl 2.8, $CaCl_2$ 1, $MgCl_2$ 2, HEPES 10, glucose 10, and the pH was adjusted to 7.2 with NaOH. Iso1 and Iso2 intracellular pipette-filling buffer contained (in mM) $K^+$-Glu 140, NaCl 8, HEPES 10, and the pH was adjusted to 7.2. TRPM7 intracellular pipette-filling buffer contained (in mM) $Cs^+$-Glu 140, NaCl 8, HEPES 10, $Cs^+$-BAPTA 10, the pH being adjusted to 7.2 with CsOH. The final osmolarity of each of the above buffers was ~300 mOsm.

### Mag-fura 2-assisted intracellular $Mg^{2+}$ measurements/$Mg^{2+}$ influx

Cells were loaded with mag-fura 2 as described in Kolisek et al. [17]. Measurements were performed in HBSS medium at 37 °C in 3-ml cuvettes containing 2-ml cell suspension under stirring. $MgCl_2$ was added stepwise to final concentrations of 1, 3, and 10 mM. The 340/380-nm ratios were acquired with the spectrofluorometer LS55 (PerkinElmer) by using the fast filter accessory operated

by FL WinLab version 4.00.03 (PerkinElmer). Intracellular $Mg^{2+}$ concentrations were calculated as described in Kolisek et al. [17].

### Mag-fura 2-assisted intracellular $Mg^{2+}$ measurements/$Mg^{2+}$ efflux

Cells for $Mg^{2+}$ efflux measurements were loaded with mag-fura 2 and $Mg^{2+}$ as described in Kolisek et al. [18, 20]. Measurements were performed in HBSS medium at 37 °C in 3-ml cuvettes containing 2-ml cell suspension under stirring. The duration of efflux measurements was set to 20 min. The 340/380 nm ratios were acquired with the spectrofluorometer LS55 (PerkinElmer) by using the fast filter accessory operated by FL WinLab version 4.00.03 (PerkinElmer). Intracellular $Mg^{2+}$ concentrations were calculated as described in Kolisek et al. [18, 20].

### Determination of total cellular Mg concentration ($[Mg]_t$) by DCHQ5-spectrofluorometry

Fluorometric measurements were made by using the spectrofluorometer LS55 (PerkinElmer). The excitation wavelength was set to 360 nm, and the emission wavelength interval was set from 400 to 650 nm. The phenyl derivative of the diaza-18-crown-6 hydroxyquinoline probe (DCHQ5) was dissolved to give a concentration of 1.37 mM in dimethylsulfoxide. The final concentration of the fluorophore used for the fluorometric experiments was 15 μM. The calibration curve was established as described in Sargenti et al. [35], and $[Mg]_t$ of samples was determined by linear regression analysis.

The samples were prepared as follows: cells were trypsinized (Perbio Science) and centrifuged; pellets were rinsed three times with HBSS supplemented with 1 mM $MgCl_2$ (37 °C). Cells were divided into four treatment groups: (1) cells were rinsed with HBSS (37 °C), resuspended in the same solution, and sonicated at time 0 min; (2) cells were incubated for 10 min in HBSS supplemented with 10 mM $MgCl_2$ (37 °C), rinsed with HBSS (37 °C), resuspended in the same solution, and sonicated; (3) cells were incubated for 30 min in HBSS supplemented with 10 mM $MgCl_2$ (37 °C), rinsed with HBSS (37 °C), resuspended in the same solution, and sonicated; (4) cells were incubated for 30 min in HBSS supplemented with 10 mM $MgCl_2$ (37 °C) and subsequently for 10 min in $Mg^{2+}$-free HBSS (37 °C), rinsed, resuspended in the same solution, and sonicated. The amount of protein in each sample was detected by using the Pierce 660-nm protein assay reagent (Pierce Biotechnology). Samples containing 25 μg protein each were used for the measurement of $[Mg]_t$.

### Strep-affinity chromatography and Western blotting

Cells were solubilized in lysis buffer (100 mM Tris-HCl, pH 7.8; 150 mM NaCl; 1.2 % Triton X-100, cOmplete Mini protease inhibitor cocktail (Roche Diagnostics)) for 30 min on ice. After centrifugation (20 min, 14,000 rpm, 4 °C) to remove non-solubilized material, the Triton concentration was reduced to 1 % by dilution with lysis buffer without Triton. Samples were loaded onto a column packed with Strep-Tactin resin (Qiagen). The column was washed twice with wash buffer (100 mM Tris-HCl, pH 7.8; 150 mM NaC; 0.8 % Triton X-100) and bound proteins were eluted in the same buffer but with D-desthiobiotin at a final concentration of 2.5 mM.

For detection of CNNM2 with an anti-Strep antibody or with an antibody directed against native CNNM2, protein samples were run on 5 or 10 % SDS-polyacrylamide (PAA) gels (as indicated) and electroblotted to a polyvinylidene difluoride (PVDF) membrane. After being blocked (5 % milk in TBS-T, 2 h) membranes were incubated with the primary Ab. An anti-CNNM2 Ab (Abgent, 1:1000 in 2.5 % milk in TBS-T) or an Ab directed against the Strep-tag (Qiagen, 1:1000 in 2.5 % milk in TBS-T) was used as the primary antibody. A horseradish peroxidase (HRP)-conjugated anti-rabbit secondary Ab (1:2000, Cell Signaling Technology) was used in combination with the Ab recognizing native CNNM2, and an HRP-conjugated anti-mouse secondary Ab (1:1000, Cell Signaling Technology) was used for the anti-Strep Ab. For standard Western blots, PageRuler™ prestained protein ladder, PageRuler Plus™ prestained protein ladder, and/or Spectra™ multicolor broad-range protein ladder (all Thermo Fisher Scientific) were used for size estimation and to control the efficiency of protein transfer from the gel to the PVDF membrane.

### Blue native Western analysis of Iso1 and Iso2 complex-forming abilities

Detection of high molecular weight complexes by blue native electrophoresis and Western blot with an Ab directed against the native epitope of CNNM2 were performed as follows. Cells were harvested, washed twice in ice-cold PBS, and resuspended in lysis buffer containing (in mM) Tris-HCl pH 7.8, NaCl 150, 1.2 % Triton X-100, and cOmplete ULTRA protease inhibitor (Roche Diagnostics). Native lysis was performed for 20 min at 4 °C with gentle agitation followed by a clarifying spin (20 min, 14,000 rpm, 4 °C). The supernatant was separated on a native 5–18 % PAA gradient gel, and blue native electrophoresis was performed according to Schägger and von Jagow [36]. The calibration standards used in BN-PAGE (NativeMark™ Unstained Protein Standard, Invitrogen) were IgM hexamer (1236 kDa), IgM pentamer (1048 kDa), apoferritin band 1 (720 kDa), apoferritin band 2

(480 kDa), B-phycoerythrin (242 kDa), lactate dehydrogenase (146 kDa), bovine serum albumin (66 kDa), and soybean trypsin inhibitor (20 kDa). The marker lane was cut from the remaining gel and stained with Coomassie brilliant blue. Following electrophoresis, semi-dry blotting to a PVDF membrane was performed at 100 V for 1 hr. A rabbit Ab directed against CNNM2 (Abgent) was used in combination with a secondary anti-rabbit antibody (Cell Signaling Technology) to detect CNNM2-containing protein complexes. Proteins were visualized by use of the SuperSignal™ West Pico system (Pierce Biotechnology).

### Iso1 and Iso2 membrane topology/functional assay and SU-YTHa

Briefly, the bait (*Iso1 and Iso2*) was inserted into the vectors p*BT3-STE* and p*BT3-N* (both Dualsystems Biotech) via the *Sfi*I(A) and *Sfi*I(B) restriction sites. Insertion led to the generation of a DNA template for the C- or N-terminal fusion of *Iso1* and *Iso2* with the *Cub-LexA-VP16* reporter cassette. The orientation and the sequence of the inserts were verified by 5′- and 3′-end sequencing. Plasmids containing bait constructs were respectively inserted into *Saccharomyces cerevisiae* reporter strain NMY32 (Dualsystems Biotech) and coexpressed with several positive controls [27]. The p-*BT3-STE-Iso1* and p-*BT3-STE-Iso2* were suitable for downstream experimentation. Human kidney cDNA library P00226 (Dualsystems Biotech) was cloned into p*PR3-N* (Dualsystems Biotech). The estimated complexity of the library was $2.6 \times 10^6$ and the average insert size was 1.8 kb. The library was inserted into strain NMY32 bearing the bait constructs, and yeasts were grown on SD −ade, −his, −leu, −trp, supplemented with 3-aminotriazole (2.5 mM for Iso1 or 5 mM for Iso2). A total of $2.6 \times 10^6$ transformants was screened for Iso1 and Iso2, respectively. Positivity of the selected clones was verified by five passages in liquid selective medium. Selected prey clones were further assayed for the activity of the second reporter, *lacZ*. Positive preys were sequenced and translated in all three reading frames. Translated sequences were blasted by using BlastX (SwissProt). The "false-positive" interactors, commonly contaminating split-ubiquitin yeast two-hybrid assay (SU-YTHa) (database of Dualsystems Biotech), were excluded from the final evaluation.

### Statistics

(1) Two-tailed Student's *t* test was used to compare differences between two means (i.e., GED at 0 h and GED at respective time points for each MRG (Table 1; Supplemental Tab. 1)). (2) A post hoc Holm Sidak 2-factor ANOVA was used to compare 2-factorial datasets (i.e., $\Delta\ [Mg^{2+}]_i$ tet(−/+) × Iso(1/2) at particular $[Mg^{2+}]_e$ (Table 2; Table 3)). (3) A post hoc Holm Sidak 3-factor ANOVA was used to compare 3-factorial datasets (i.e., $[Mg]_t$ tet(−/+) × Iso(1/2) × interventions (Fig. 8)). A Shapiro-Wilk normality test was used for (2) and (3). Data are presented as means ± SE. Differences of $P < 0.05$ were considered significant. Statistical analyses were executed by using SigmaPlot 11.0 (Systat Software, Inc.).

**Table 1** *CNNM2* expression's $C_T$ difference (GED ± SE) monitored at indicated time points in JVM-13 and Jurkat cells incubated in nominally $Mg^{2+}$-free medium

| | JVM-13/*CNNM2* | | | | Jurkat/*CNNM2* | | | |
|---|---|---|---|---|---|---|---|---|
| Time (h) | GED | SE | N/n | *P* value | GED | SE | N/n | *P* value |
| 3 | 0.64 | 0.37 | 3/9 | 0.42 | 0.48 | 0.32 | 3/9 | 0.55 |
| 5 | 2.82 | 0.25 | 3/9 | 0.01 | 0.56 | 0.31 | 3/9 | 0.48 |
| 8 | 3.45 | 0.32 | 3/9 | 0.01 | 0.73 | 0.40 | 3/9 | 0.43 |
| 12 | 8.18 | 0.28 | 3/9 | 0.001 | 0.97 | 0.29 | 3/9 | 0.23 |
| 24 | 7.08 | 0.35 | 3/9 | <0.01 | 1.67 | 0.33 | 3/9 | 0.09 |
| 48 | 9.94 | 0.69 | 3/9 | <0.05 | 2.65 | 0.30 | 3/9 | <0.05 |

*N* sum of independent biological experiments, *n* sum of repetition performed within *N*; *P P* value

## Results

### Severe $Mg^{2+}$ starvation induces overexpression of CNNM2 in JVM-13 and Jurkat cells

First, we wondered whether *CNNM2* reacted to severe $Mg^{2+}$ starvation at the transcription level. We decided to test this in JVM-13 and Jurkat cells, which are derived from cell types normally exposed to changes of $[Mg^{2+}]$ in blood. The 48-h monitoring of *CNNM2* expression in JVM-13 and Jurkat cells, which were bathed in medium nominally free of $Mg^{2+}$ revealed that (1) JVM-13 cells overexpressed *CNNM2* (GED >1) as early as 3 to 5 h after the beginning of the $Mg^{2+}$ starvation period, and GED increased with time, reaching a maximum of approximately 10 at 48 h after the beginning of starvation (Fig. 1a; Table 1); (2) Jurkat cells overexpressed *CNNM2* (GED >1) at 12 to 24 h after the beginning of $Mg^{2+}$ starvation, and GED increased with time, reaching a maximum of approximately 2.7 at 48 h after the beginning of starvation (Fig. 1b; Table 1). Therefore, Jurkat cells overexpressed *CNNM2* with a later onset than did JVM-13 cells, and the maximal averaged GED determined in Jurkat cells was only ~27 % of that in JVM-13 cells (Table 1). In comparison with JVM-13 cells, only a poor transcription response was observed for all the tested *MRG*s in Jurkat cells (Fig. 1a vs. 1b; Supplemental Tab. 1).

**Table 2** $\Delta[Mg^{2+}]_i$ calculated from the difference between $[Mg^{2+}]_i$ measured after addition of $Mg^{2+}$ to the bath solution ($[Mg^{2+}]_e = 1$ or 3 or 10 mM) and the basal $[Mg^{2+}]_i$ detected at $[Mg^{2+}]_e = 0$ mM

| tet | CNNM2/ Iso | N | $\Delta [Mg^{2+}]_i$ $^{(1-0)}$ ± SE (mM) | $\Delta [Mg^{2+}]_i$ $^{(3-0)}$ ± SE (mM) | $\Delta [Mg^{2+}]_i$ $^{(10-0)}$ ± SE (mM) |
|---|---|---|---|---|---|
| − | 1 | 16 | 0.04 ± 0.01 | 0.11 ± 0.02 | 0.23 ± 0.04 |
| + | 1 | 16 | 0.04 ± 0.01 | 0.10 ± 0.02 | 0.19 ± 0.03 |
| − | 2 | 16 | 0.04 ± 0.01 | 0.12 ± 0.03 | 0.26 ± 0.07 |
| + | 2 | 15 | 0.05 ± 0.01 | 0.12 ± 0.02 | 0.24 ± 0.04 |

*Iso* isomorph, *N*, sum of independent biological experiments, *tet* tetracycline

## Characterization of the transgenic expression system

Functional examination of both variants was performed in the newly generated HEK293 cell lines with the tet-regulated expression of stably transfected HA-Strep-Iso1 and HA-Strep-Iso2. A robust inducible expression was detected by Western blot analysis for both Iso1 and Iso2, respectively, when the blots were immunodecorated with an antibody against native CNNM2 (Fig. 2a). The antibody against native CNNM2 yielded several signals, except of the monomer (97 kDa), putatively arising from degradation products or protein modifications (e.g., glycosylation) [7]. When we performed Western blot detection with an Ab directed against the Strep-tag, we identified only faint signals corresponding to Iso1 and Iso2 bands (~100 kDa) in +tet cells, and no Iso1- and Iso2-specific signals were detected in −tet cells (Fig. 2b). Strep-affinity purification of the Strep-tagged Iso1 and Iso2, however, allowed the visualization of the Iso1- and Iso2-specific bands in induced cells (Fig. 2c). Where indicated, we also used HEK-293 cells transiently expressing CNNM2 Iso1 or Iso2, both with a C-terminal Strep-His-tag (Fig. 3a–d). Expression of Iso1 and Iso2 with a C-terminal tag resulted in markedly stronger signals in Western blot. In addition to the signal for monomeric CNNM2, a signal with a molecular weight higher than ~260 kDa was detected (Fig. 3a), which indicated the ability of CNNM2 to form strong protein-protein interactions that were not dissolved in the presence of SDS and reducing agents.

## CNNM2 Iso1 and Iso2 exhibit dispersed cellular localization

The cellular localization of CNNM2 and/or its isomorphs is still controversial. Therefore, we examined the cellular distribution of both variants of CNNM2 in transgenic HEK293 cells. As full-sized N-terminally-Strep-tagged Iso1 and Iso2 could be detected on Western blots (Fig. 2b, c), we decided to perform confocal imaging and to examine the pattern of the cellular distribution of both N-terminally tagged isomorphs. As shown in Fig. 4, we were able to detect N-terminally Strep-tagged Iso1- and Iso2-specific signals corresponding to "full-sized" Iso1 or Iso2, or to the cleaved N-terminal flanking region and TM1 of Iso1 and Iso2, or to both. The Iso1 signal had a clearly different pattern of distribution (Fig. 4a, b) from the signal of Iso2 (Fig. 4c, d). Next, we immunodecorated Iso1 and Iso2 with a polyclonal Ab directed against the native epitope of CNNM2, which is present in both variants. Figure 5a–d shows that the Ab recognized CNNM2 in −tet cells and in significantly higher quantities in +tet cells. Moreover, as this figure (Fig. 5) makes obvious, both tested CNNM2 isomorphs were dispersed throughout the various intracellular compartments in both −tet and +tet cells. Finally, we performed immunofluorescence imaging on the cells transiently transfected with C-terminally tagged Iso1-Strep and Iso2-Strep (Figs. 6a–e and 7a–e). Both C-terminal-tagged variants exhibited a dispersed cellular distribution poorly overlapping with the predominantly mitochondrial COXIV signal. In agreement with the latter, the

**Table 3** $\Delta[Mg^{2+}]_i$ calculated from the difference between $[Mg^{2+}]_i$ measured in $Mg^{2+}$-preloaded −tet and +tet Iso1 and Iso2 at the beginning ($T_{0\ min}$) of the measurements and $[Mg^{2+}]_i$ at the end of the measurements ($T_{20\ min}$) in $Mg^{2+}$-free HBSS

| tet | CNNM2/Iso | N | $\Delta [Mg^{2+}]_i$ $^{(T20-T0\ min)}$ ± SE (mM) |
|---|---|---|---|
| − | 1 | 5 | 0.02 ± 0.02 |
| + | 1 | 5 | 0.02 ± 0.01 |
| − | 2 | 5 | 0.01 ± 0.01 |
| + | 2 | 5 | 0.01 ± 0.02 |

*Iso* isomorph, *N* sum of independent biological experiments, *tet* tetracycline

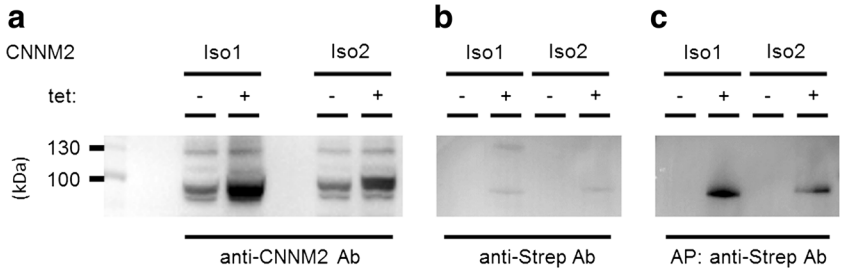


**Fig. 2** Immunodetection of N-terminally Strep-HA-tagged CNNM2 Iso1 and Iso2 in total protein (**a**, **b**) and Strep-affinity-purified (**c**) −tet and +tet isolations. HEK293 cells stably transfected with N-terminally Strep-tagged CNNM2 Iso1 or Iso2 were tet-induced (24 h) and lysed under denaturing conditions and proteins were separated by SDS-PAGE. The Ab directed against the C-terminus of native CNNM2 (**a**) or against N-terminal Strep-tag (**b**) were used for immunodetection. Immunodetection of Iso1 and Iso2 in Strep-affinity-purified isolations from +tet and −tet cells with antinative CNNM2 Ab is shown in panel **c**. PageRuler™ prestained protein ladder was used for size estimation and to control the efficiency of protein transfer from the gel to PVDF membrane. Abbreviations: *Ab*, antibody; *AP*, affinity-purified; *Iso*, isomorph; *kDa*, kilo-Dalton; *tet*, tetracycline

3D imaging (Supplemental Movie 1) also showed that the signal of immunodecorated Iso1-Strep (anti CNNM2 Ab) did not colocalize with the MitoTracker Green FM signal. Therefore, both variants of CNMM2 are most probably not proteins primarily targeted to mitochondria. In contrast to Iso1 and Iso2, Iso1-Strep and Iso2-Strep were not detected in the nuclear compartment (Figs. 5b, d vs. 6d and 7d). This can be explained by the higher specificity of monoclonal anti-Strep Ab when compared with the specificity of polyclonal anti-CNNM2 Ab.

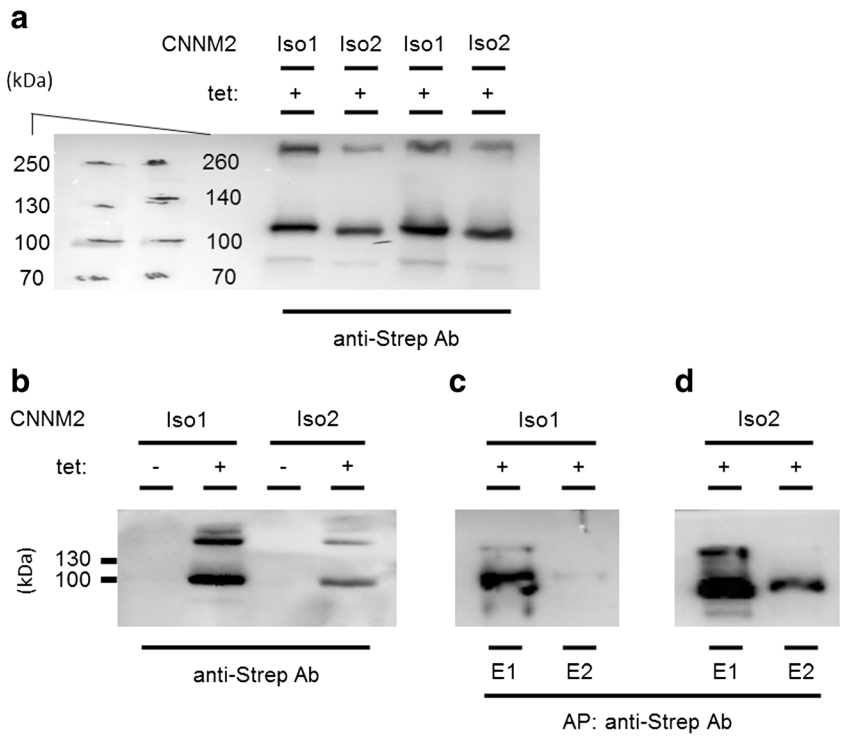


**Fig. 3** Immunodetection of C-terminally Strep-His-tagged CNNM2 Iso1 and Iso2 in total protein isolations and elution fractions after affinity chromatography from transiently transfected HEK293 cells. Cells were transiently transfected with pcDNA5/TO carrying either CNNM2 Iso1 or Iso2. Protein expression was induced 24 h after transfection by addition of tet (24 h, +tet). Transfected control cells remained untreated (−tet). Cells were lysed and crude protein extracts were either directly separated by SDS-PAGE (**a**, **b**) or Strep-affinity chromatography was performed and the elution fractions were loaded onto the gel (**c**, **d**). Longer SDS-PAGE (**a**; 1 h 45 min, 5 % PAA gel) and shorter SDS-PAGE (**b**–**d**; 1 h 20 min, 10 % PAA gel) were performed. The Ab directed against the C-terminal Strep-tag was used for immunodetection. PageRuler Plus™ prestained protein ladder and/or Spectra™ multicolor broad-range protein ladder were used for size estimation and to control the efficiency of protein transfer from the gel to PVDF membrane. Abbreviations: *Ab*, antibody; *AP*, affinity-purified; *E*, elution fraction; *Iso*, isomorph; *kDa*, kilo-Dalton; *tet*, tetracycline

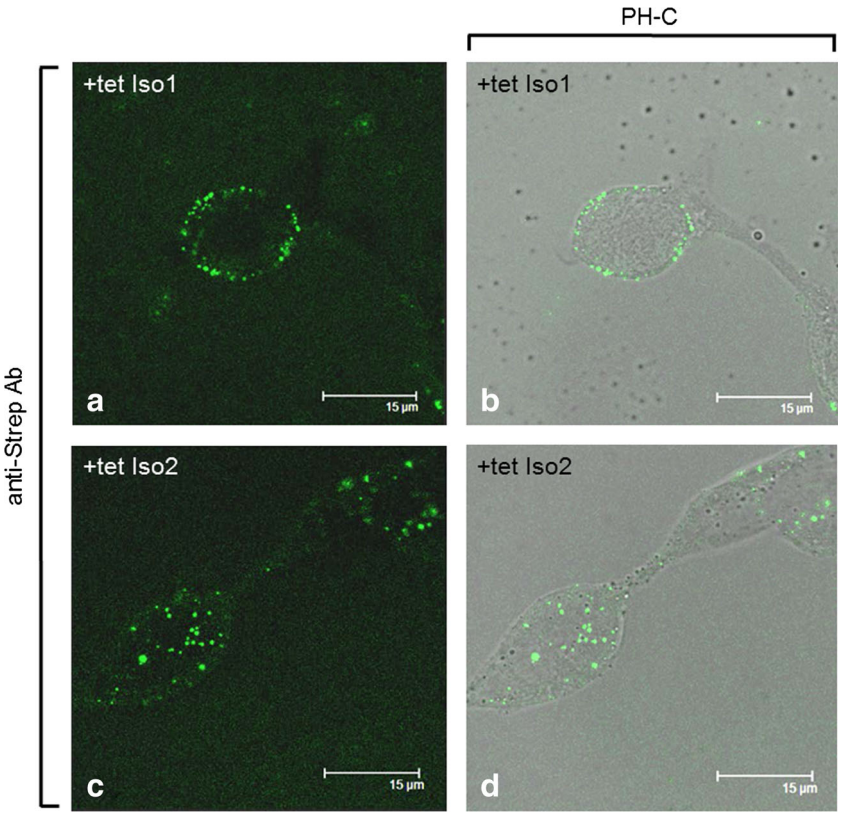


**Fig. 4** Immunofluorescence detection of N-terminally Strep-tagged Iso1 (**a**, **b**) and Iso2 (**c**, **d**) in +tet Iso1 and Iso2 cells. *Bar* indicates 15 µm in each panel. The N-terminally Strep-tagged Iso1 and Iso2 were immunolabeled with primary mouse anti-Strep Ab and secondary goat anti-mouse Ab conjugated with Alexa-Green 488. Abbreviations: *Ab*, antibody; *Iso*, isomorph; *PH-C*, phase-contrast; *tet*, tetracycline

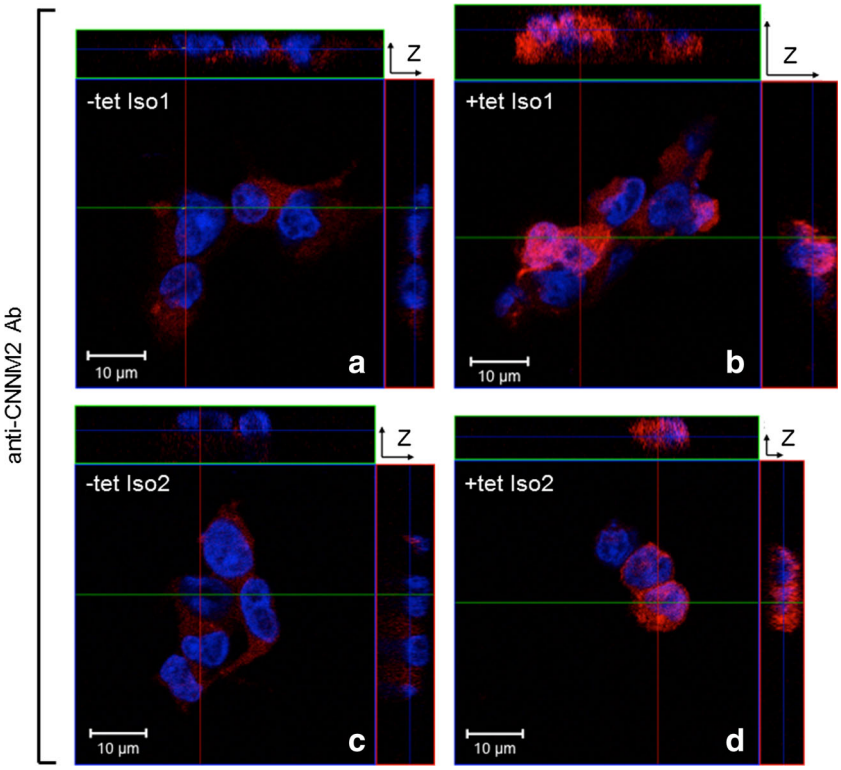


**Fig. 5** Immunofluorescence detection of Iso1 and Iso2 in −tet Iso1 (**a**) and −tet Iso2 (**c**), and in +tet Iso1 (**b**) and +tet Iso2 (**d**) cells. *Bar* indicates 10 µm in each panel. The Iso1 and Iso2 were immunolabeled with primary rabbit polyclonal Ab directed against the native CNNM2 epitope (AA575–AA625) and secondary goat anti-rabbit Ab conjugated with Alexa-Red 594. Nuclei were stained with DAPI. Abbreviations: *Ab*, antibody; *DAPI*, 4′,6-diamino-2-phenylindol; *Iso*, isomorph; *tet*, tetracycline

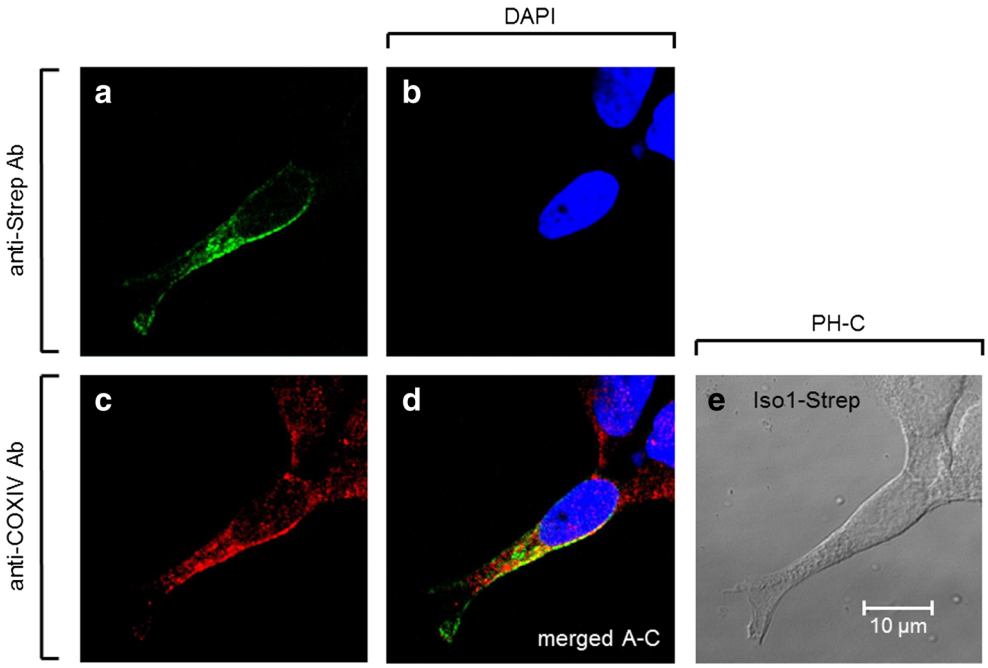


**Fig. 6** Coimmunostaining of C-terminally Strep-tagged Iso1 and of COXIV in +tet Iso1-Strep cells. **a** Iso1-Strep immunodecorated with primary mouse anti-Strep Ab and secondary goat anti-mouse Ab conjugated with Alexa-Green 488; **b** nuclei were stained with DAPI; **c** COXIV immunodecorated with primary rabbit anti-COXIV Ab and secondary goat anti-rabbit Ab conjugated with Alexa-Red 594; **d** merged image (*A–C*); **e** PH-C, bar indicates 10 μm. Abbreviations: *Ab*, antibody; *COXIV*, cytochrome oxidase c IV; *DAPI*, 4′,6-diamino-2-phenylindol; *Iso*, isomorph; *PH-C*, phase contrast; *tet*, tetracycline

## Iso1 and Iso2 do not transport $Mg^{2+}$ per se

In our previous study, we demonstrated that Iso1 (but not Iso2) was able to complement the $Mg^{2+}$-dependent growth deficiency of *S. enterica* sv. *Typhimurium* strain MM281, which is lacking in all three major $Mg^{2+}$-transport mechanisms, namely CorA, MgtA, and MgtB [40]. Therefore, we assumed that human Iso1 was able to transport $Mg^{2+}$ when expressed in bacteria. However, the possibility that the $Mg^{2+}$ transport was the redundant function of Iso1 seen only in a heterologous (bacterial) system was not ruled out. Stuiver et al. have reported that CNNM2 mediate $Mg^{2+}$-sensitive $Na^{+}$ currents [41]. Therefore, we assessed whether Iso1 and Iso2 were able to generate measurable $Na^{+}$ or $Mg^{2+}$ currents. As a reference, we used TRPM7 inducibly expressed in HEK293 cells, which unequivocally acts as a channel permeable for divalent ions [24, 26], and established experimental conditions suitable for the assessment of the electrogenic transport

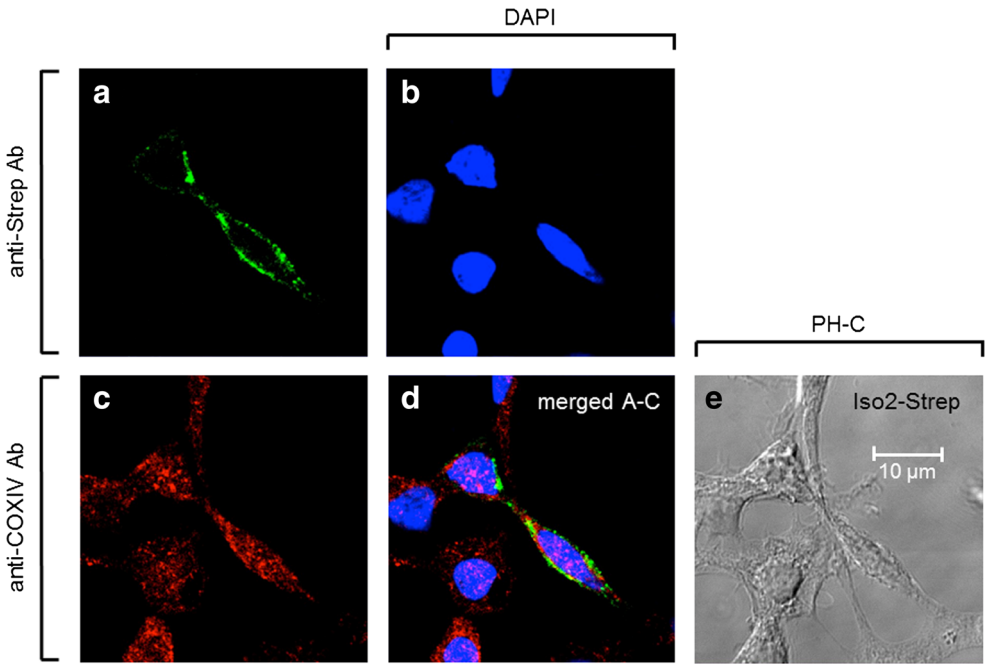


**Fig. 7** Coimmunostaining of C-terminally Strep-tagged Iso2 and of COXIV in +tet Iso2-Strep cells. **a** Iso2-Strep immunodecorated with primary mouse anti-Strep Ab and secondary goat anti-mouse Ab conjugated with Alexa-Green 488; **b** nuclei were stained with DAPI; **c** COXIV immunodecorated with primary rabbit anti-COXIV Ab and secondary goat anti-rabbit Ab conjugated with Alexa-Red 594; **d** merged image (*A–C*); **e** PH-C, *bar* indicates 10 μm. Abbreviations: *Ab*, antibody; *COXIV*, cytochrome oxidase c IV; *DAPI*, 4′,6-diamino-2-phenylindol; *Iso*, isomorph; *PH-C*, phase-contrast; *tet*, tetracycline

of $Mg^{2+}$ through bona fide $Mg^{2+}$-permeable ion channels. Figure 8a illustrates the characteristic constitutive activity of TRPM7 currents at the time of break-in, followed by the temporal activation of TRPM7 inward and outward currents when perfusing cells with intracellular solutions that lack Mg·ATP [24, 26]. Based on the composition of external and internal solutions (see "Material and methods" section), the inward currents at −80 mV are carried by $Ca^{2+}$ and outward currents at +80 mV by $Cs^{+}$. After full activation of TRPM7, the $Mg^{2+}$-free external solution was replaced by isotonic $MgCl_2$, revealing a brief but discernible increase in inward current at −80 mV caused by $Mg^{2+}$ entry that was followed by the strong inhibition of currents at all voltages because of the $Mg^{2+}$-dependent inhibition of TRPM7 by intracellular $Mg^{2+}$ [26]. High-resolution current-voltage (I-V) relationships obtained by the voltage ramp protocol used to monitor membrane currents before and immediately after switching to isotonic $MgCl_2$ demonstrated a significant increase in inward current and a shift in reversal potential (Fig. 8b), consistent with enhanced $Mg^{2+}$ currents through TRPM7 channels [24, 26]. We next applied the same experimental protocol to HEK293 cells overexpressing Iso1 and Iso2 (Fig. 8c–f). In contrast to a previous report [41] and despite significant levels of overexpressed Iso1 and Iso2, neither of the isoforms exhibited large constitutive membrane currents above the control. Initially, cells exhibited small basal currents consistent with the resting endogenous TRPM7 current that experienced a relatively small increase mostly in outward current (Fig. 8c–f), but these currents were consistent with endogenously expressed TRPM7 [14]. Upon switching to isotonic $MgCl_2$ solution, no significant inward current was detectable. Instead, both inward and outward currents were inhibited as expected because of the $Mg^{2+}$-dependent inhibition of endogenous TRPM7 channels. Given the very small number of TRPM7 channels expressed natively in HEK293 cells, any inward $Mg^{2+}$ current through these channels is too small to be resolved, even in the presence of isotonic $MgCl_2$. Clearly, unlike TRPM7, neither CNNM2 variant generated $Na^{+}$ or $Mg^{2+}$ currents under these conditions, despite its overexpression.

We subsequently examined the potential ability of Iso1 and Iso2 to transport $Mg^{2+}$ in a non-electrogenic mode with mag-fura 2-assisted FF-spectrofluorometry in −tet and +tet Iso1 and Iso2 cells. Additions of $Mg^{2+}$ to HBSS medium to give a final $[Mg^{2+}]_e$ of 1, 3, or 10 mM induced stepwise increases of the 340/380 nm mag-fura 2 ratio and $[Mg^{2+}]_i$ in −tet and +tet Iso1 and Iso2 cells (Table 2, Supplemental Fig. 1). However, the differences between the $Mg^{2+}$ influx seen in induced and uninduced Iso1 and Iso2 cells were statistically insignificant (Table 2), thus indicating that the overexpression

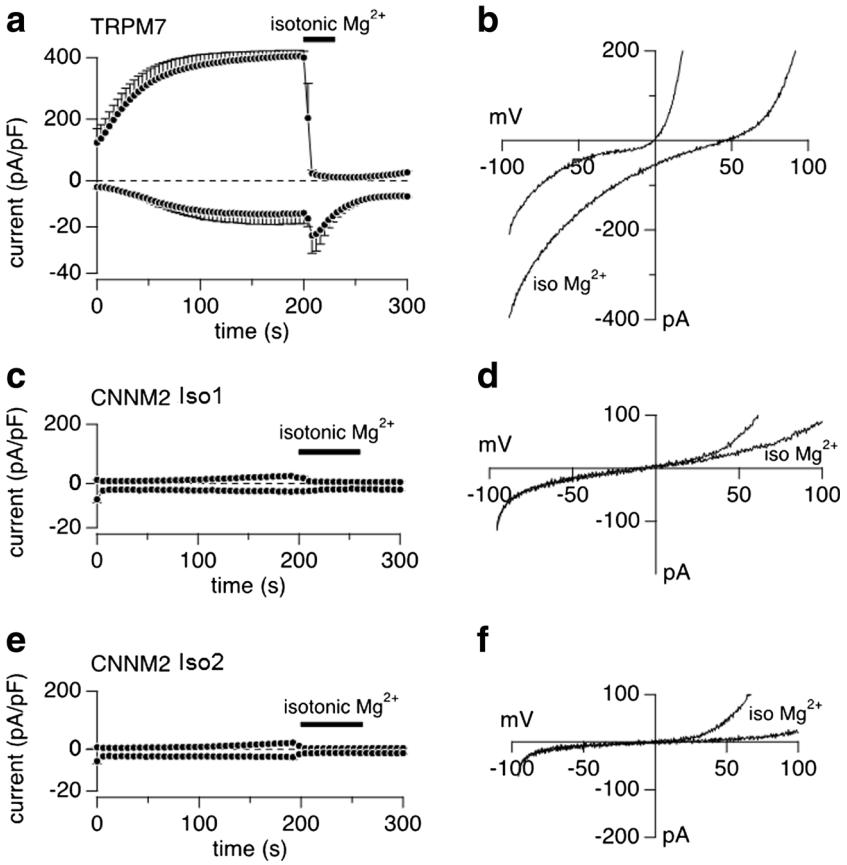


**Fig. 8** Isotonic $Mg^{2+}$ denotes extracellular application of 110 mM $MgCl_2$ (osmolarity = 316 mOsm, pH 7.4). External bath solution (in mM): 140 NaCl, 2.8 KCl, 10 Hepes, 1 $CaCl_2$, 11 glucose, pH 7.4. Internal recording solution (in mM): 140 Cs-glutamate, 8 NaCl, 10 Cs-Hepes, 10 Cs-EGTA, pH 7.2 The identical recording condition was used in current measurement in all three cell lines. **a**, **b**)Whole-cell recording of TRPM7 currents in +tet HEK293 cells ($N = 4$). **c**, **d** Currents measured in +tet Iso1 cells ($N = 6$). **e**, **f** Currents measured in +tet Iso2 cells ($N = 5$). Abbreviations: *Iso*, isomorph; *tet*, tetracycline

of Iso1 or Iso2 did not result in an increased $Mg^{2+}$ transport (influx) capacity of these cells. Moreover, no expression-related changes of basal $[Mg^{2+}]_i$ were detected between −tet and +tet Iso1 and Iso2 cells.

Supplemental Figure 2 depicts the dynamics of $Mg^{2+}$ transport (340/380 nm mag-fura 2 ratio) in −tet and +tet Iso1 and Iso2 cells and control +tet HEK293 cells overexpressing SLC41A1 [17, 18] preloaded with $Mg^{2+}$ in HBSS medium with 10 mM $Mg^{2+}$ and measured in HBSS ($Mg^{2+}$ efflux conditions). This figure reveals that the starting point of the 340/380-nm mag-fura 2 ratio in $Mg^{2+}$-preloaded control cells is markedly higher than that in −tet and +tet Iso1 and Iso2 cells, indicating that the overexpression of Iso1 or Iso2 does not increase $Mg^{2+}$ loading under our conditions when compared with −tet Iso1 or Iso2, respectively. The averaged differences between $[Mg^{2+}]_i$ measured in −tet and +tet Iso1 and Iso2 at the beginning ($T_{0\ min}$) and $[Mg^{2+}]_i$ at the end of the measurements ($T_{20\ min}$) are summarized in Table 3; the data demonstrate that overexpression of Iso1 or Iso2 does not result in an increased $Mg^{2+}$ efflux capacity of Iso1 and/or Iso2 cells. No expression-related differences of basal $[Mg^{2+}]_i$ were detected between $Mg^{2+}$-preloaded −tet and +tet Iso1 and Iso2 cells used for $Mg^{2+}$ efflux measurements.

We then used a fluorescent indicator DCHQ5 and examined whether the overexpression of Iso1 or Iso2 led to changes in total cellular Mg content. First, we determined $[Mg]_t$ in −tet and +tet Iso1 and Iso2 cells freshly transferred from cultivation (expression) medium into HBSS medium (containing 1 mM $Mg^{2+}$; $T_{0\ min}$). No differences were observed between $[Mg]_t$ measured in −tet and +tet Iso1 cells or between −tet and +tet Iso2 cells (Fig. 9). A 10- or 30-min incubation of −tet and +tet Iso1 and Iso2 cells in HBSS medium containing 10 mM $Mg^{2+}$ induced statistically insignificant changes of $[Mg]_t$ when compared with $[Mg^{2+}]_e$ 1 mM ($T_{0\ min}$) (Fig. 9). A 10-min incubation of −tet and +tet Iso1 and Iso2 cells in HBSS medium (0 mM $Mg^{2+}$) also had no effect on $[Mg]_t$ (Fig. 9). Therefore, these data indicate that Iso1 or Iso2 overexpression does not influence cellular $[Mg]_t$ at varying $[Mg^{2+}]_e$.

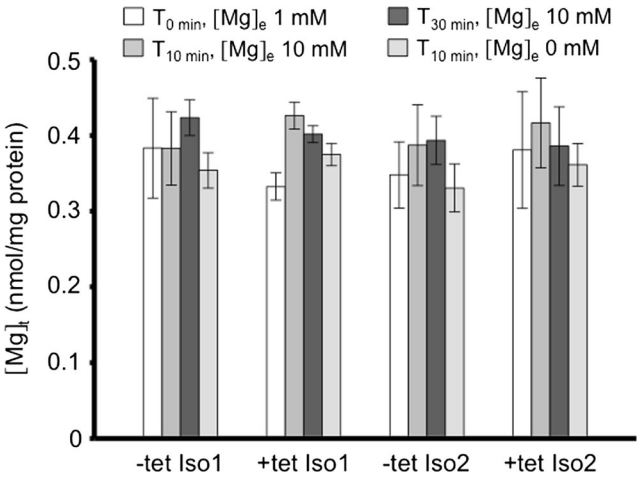


**Fig. 9** Total Mg concentrations determined by DCHQ5-spectrofluorometry in lysates of −tet and +tet Iso1 and Iso2 cells after the following pretreatments: (1) cells were lysed at $T_{0\ min}$ in medium containing 1 mM $Mg^{2+}$; (2) cells were lysed at $T_{10\ min}$ after incubation in medium containing 10 mM $Mg^{2+}$; (3) cells were lysed at $T_{30\ min}$ after incubation in medium containing 10 mM $Mg^{2+}$; (4) $Mg^{2+}$-preloaded cells (30 min in medium containing 10 mM $Mg^{2+}$) were lysed at $T_{10\ min}$ after incubation in $Mg^{2+}$-free medium. For each treatment group, $N = 3$. Abbreviations: *DCHQ5*, phenyl derivative of the diaza-18-crown-6 hydroxyquinoline probe; *Iso*, isomorph; *tet*, tetracycline

## Iso1 and Iso2 form protein complexes and have distinctive divergent spectra of interactors

We next tested the ability of Iso1 and Iso2 to form protein complexes. Results of blue native electroseparation suggested that both Iso1 and Iso2 formed protein complexes in vivo (Fig. 10). After immunoblotting with an Ab directed against native CNNM2, we detected three signals (C3, C4, C5) between the 242-kDa and the 480-kDa marker bands and additional protein complexes with a molecular weight of approximately 550–600 kDa (C2) and 720 kDa (C1) for both Iso1 and Iso2 (Fig. 10a). When we lowered the amount of total native protein, we were able to resolve a strong signal of C4 and to demonstrate that C4 consisted of two complexes, the C4.1 with a higher molecular weight and the C4.2 with a lower molecular weight (Fig. 10b). To examine the spectra of Iso1 and Iso2 interactors in vivo and to determine the possible function(s) of both isomorphs, we performed SU-YTHa. We first completed the split-ubiquitin functional assay and identified Iso1 and Iso2 fused C-terminally with the Cub-LexA-VP16 reporter moiety as a suitable bait construct for the downstream SU-YTHa assay (Supplemental Fig. 3). This also confirmed the proposed orientation of the N- and C-termini in "de Baaij's model" of CNNM2 membrane topology [7]. As bait, we used a human kidney-derived cDNA library (NubG-fused). Results of our screen are summarized in Supplemental Tables 2 and 3. The spectrum of unique binding candidates of Iso1 involved only six proteins. However, the spectrum of potential interactors identified for Iso2 was much larger, accounting for 50 different proteins. All candidate proteins in both Iso1 and Iso2 screens were identified as singletons.

As the only common interactor of both Iso1 and Iso2, we identified spectrin β chain (Brain) 1 (SPTBN1; UniProt ID Q01082) in two independent screens. As other interactors of Iso1, we identified $Mg^{2+}$-dependent enzyme isopentenyl-diphosphate delta isomerase 1 (IDI1; Q13907) [12], interferon regulatory factor 2 binding protein 2 (IRF2BP2; Q7Z5L9), SERPINE1 MRNA binding protein 1 (SERBP1; Q8NC51), coiled-coil-helix-coiled-coil-helix domain containing 7 (CHCHD7; Q9BUK0), and Parkinson Protein 7 (PARK7/DJ-1; Q99497; multifactorial protein, when mutated involved in the pathophysiology of Parkinson's disease (PD) and

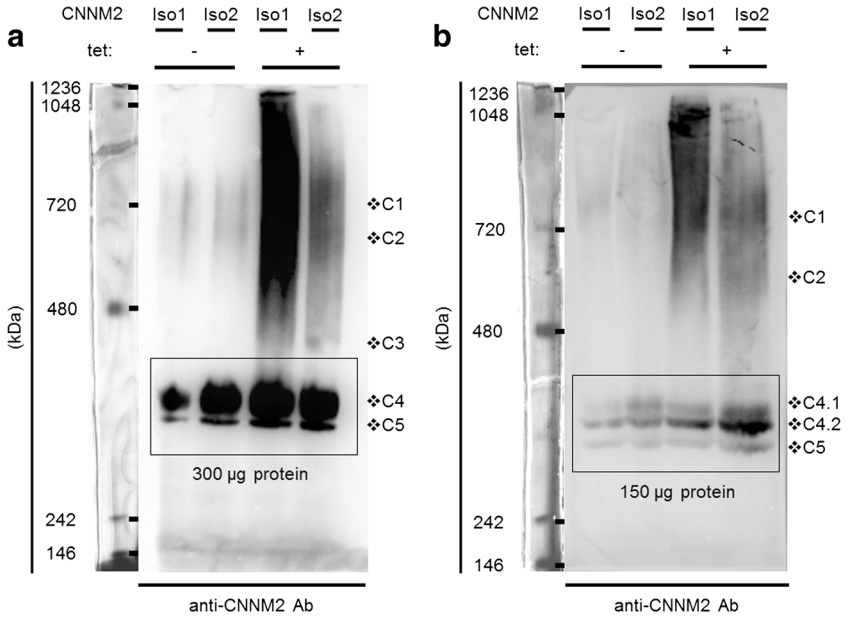


**Fig. 10** Complex-forming ability of CNNM2 isoforms. +tet Iso1 or Iso2 cells together with the respective controls (−tet Iso1 and Iso2 cells) were solubilized under native conditions and separated on a native polyacrylamide 8–15 % gradient gel. The Ab recognizing CNNM2 native epitope was used for immunodetection in combination with an HRP-conjugated secondary antibody. In **a**, samples with a final amount of 300 µg were loaded on the gel. Final amount of the total protein loaded on the gel depicted on **b**was 150 µg. *C* indicates Iso1- and/or Iso2-specific complexes. Abbreviations: *Iso*, isomorph; *C*, complex; *kDa*, kilo-Dalton; *tet*, tetracycline

cancerogenesis). These Iso1 interactors (Supplemental Tab. 2) are proteins localized in (or associated with) the nucleus, cytoplasm, cytoplasmic membrane, mitochondria, and peroxisomes (Fig. 11a, http://www.uniprot.org). Functionally, they are involved in processes such as scaffolding and cellular architecture, autophagy, cholesterol biosynthesis, and RNA and DNA metabolism (Fig. 11b, http://www.uniprot.org).

Among the potential Iso2 interactors, we identified proteins with various cellular localizations (Supplemental Tab. 3, Fig. 11a, http://www.uniprot.org). These are involved in a markedly broader scale of cellular processes (apoptosis, autophagy/mitophagy, cell cycle, cell proliferation, cell growth, coenzyme Q10 biosynthesis, cell architecture/cytoskeleton, cell differentiation, RNA and DNA metabolism, glycolysis, glucosaminoglycans biosynthesis, immunity, solute transport, protein biosynthesis, tight junctions/cell junctions; Fig. 11b, http://www.uniprot.org) than the interactors of Iso1. In particular, further examination of the interaction between Iso2 and PD-associated PTEN-induced putative kinase 1 (mitochondrial serine/threonine-protein kinase PINK1; Q9BXM7), the interaction between Iso2 and Parkin-binding isoform 5 of activating molecule in BECN1-regulated autophagy protein 1 (AMBRA1; Q9C0C7), and the interaction between Iso2 and brain protein 44-like protein (also known as mitochondrial pyruvate carrier 1 (MPC1); Q9Y5U8) associated with autosomal recessive mitochondrial pyruvate carrier deficiency [4] might be relevant for clarifying the role of disturbed IMH in chronic and degenerative diseases.

## Discussion

The number of human and animal diseases that are associated with imbalanced extracellular $Mg^{2+}$ homeostasis and IMH is constantly growing. Among these are prominent ailments such as *diabetes mellitus* type 2, ischemic heart disease, essential hypertension, Alzheimer's disease (AD) and PD, amyotrophic lateral sclerosis (ALS), and various psychiatric disorders [2, 15, 21, 28]. Little is known about the molecular mechanisms that might be responsible for hypomagnesemia and intracellular $Mg^{2+}$ deficiency in these diseases.

CNNM2 is a distant partial homolog of bacterial $Mg^{2+}$ transporter CorC [40]. Its mutated variant has been associated with severe hypomagnesemia in Man [41]. Goytain and Quamme have demonstrated that restricted $Mg^{2+}$ intake leads to overexpression of *CNNM2* in mouse model [10, 31]. CNNM2 has also been associated with the regulation of serum Mg concentrations [23]. In agreement with the latter is the inducibility of *CNNM2* overexpression in JVM-13 and Jurkat cells by severe $Mg^{2+}$ starvation. Indeed, our data further substantiate the involvement of *CNNM2* in the cellular response to changing $[Mg^{2+}]_e$.

Noteworthy is also the high-expression responsiveness of other *MRGs* (formerly described by the group of Quamme in mice [31]) to $Mg^{2+}$ depletion in JVM-13 cells (Fig. 1a). Surprisingly, the expression response of *CNNM2* (and also of other *MRGs*) in Jurkat cells markedly differs from that in JVM-13 cells (Fig. 1a vs. Fig. 1b). This observation leads to the conclusion that the determination of *MRG* expression in

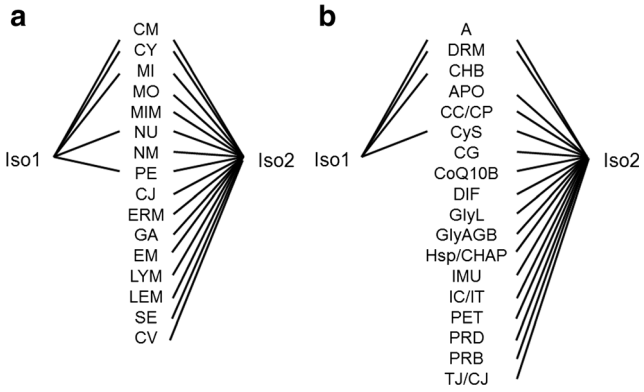


**Fig. 11** CNNM2 Iso1 and Iso2; network depicting differences between the two isoforms with respect to the cellular localizations (**a**) and the functions (**b**) of their interactors. Figure legend: **a** *CM* = cytoplasmic membrane, *CY* = cytoplasm, *MI* = mitochondria, *MOM* = mitochondrial outer membrane, *MIM* = mitochondrial inner membrane, *NU* = nucleus, *NM* = nuclear membrane, PE = peroxisome, *CJ* = cellular junction, *ERM* = endoplasmic reticulum, *GA* = Golgi, *EM* = endosomal membrane, *LYM* = lysosomal membrane, *LEM* = late endosomal membrane, *SE* = secreted, *CV* = cytoplasmic vesicles (autophagosome). **b** *A* = autophagy/mitophagy, *DRM* = DNA/RNA metabolism, *CHB* = cholesterol biosynthesis, *APO* = apoptosis, *CC/CP* = cell cycle/cell proliferation, *CyS* = cytoskeleton, *CG* = cell growth, *CoQ10B* = Coenzyme Q-10 biosynthesis, *DIF* = differentiation, *GlyL* = glycolysis, *GlyAGB* = glycosaminoglycan biosynthesis, *Hsp/CHAP* = heat shock protein/chaperone, IMU = immune response, *IC/IT* = ion channel/ion transporter, *PET* = peptide transport, *PRD* = protein degradation, *PRB* = protein biosynthesis, *TJ/CJ* = tight junction/cell junction

lymphocytes can be used as a bioindicator of intracellular $Mg^{2+}$ status, although whether *MRG* expression in primary T-lymphocytes differs from *MRG* expression in primary B-lymphocytes and lymphoblasts should be further tested. Moreover, what lies behind the poor expression responsiveness of *MRGs* to extracellular $Mg^{2+}$ depletion in Jurkat cells should be explored, as this might lead to the discovery of a general mechanism regulating not one particular component of IMH, but the whole portfolio of molecular components regulating this process.

Among all tested *MRGs*, *CNNM2* reacts at the transcriptional level to $Mg^{2+}$ depletion with the highest robustness (together with *TRPM7*). This observation also underlines a substantial involvement of *CNNM2* in the constitution and regulation of IMH.

de Baaij and coworkers have predicted that CNNM2 is a protein undergoing posttranslational ER signal peptidase cleavage of the N-terminus and the first TH [7]. Thus, in their model, the mature protein consists of three TH, an extracellularly localized N-terminus, and an intracellularly localized C-terminus [7]. Our data in Fig. 2 support the results of de Baaij and colleagues [7]. Moreover, these data also indicate that our expression system is stronger and/or more efficient than that of de Baaij et al., as we have been able to detect bands corresponding to full-sized Iso1 and Iso2 after Strep-affinity purification. The possibilities that the imperfect proteolytic maturation of Iso1 and Iso2, which might not be detectable in genetically unmodified systems, is not a simple consequence of overexpression and protein overload and that both "immature" Iso also play a role in cell physiology remain to be explored.

Wang and colleagues formerly identified human CNNM2 (ACDP2) as a nuclear protein in HeLa cells [45]. Later, Stuiver at al. localized CNNM2 in the cytoplasmic membrane of MDCK-C7 cells transiently overexpressing the protein [41]. Our confocal imaging data have shown that the N-terminally Strep-tagged Iso1 and Iso2 signal corresponding to the localization of N-terminal proteolytic breakdown product of CNNM2 maturation (Np-CNNM2) and the full-sized immature protein (iCNNM2) can be detected in both +tet Iso1 and +tet Iso2 cells (Fig. 4a–d). In the two cell lines, the fluorescent signal has a spot-like pattern indicating that NpCNNM2 and/or iCNNM2 occur in vesicular structures. Interestingly, in +tet Iso1 cells, the signal is localized primarily in the plasmalemma and/or periplasmic region, whereas in +tet Iso2 cells, the signal is scattered throughout the cell. This indicates that the maturation, sorting, targeting, and degradation of Iso1 differ from those of Iso2. Furthermore, this observation additionally supports the hypothesis that each of the Iso plays a specific role in cellular physiology. Next, in order to immunodecorate CNNM2, we used Ab directed against the native epitope of CNNM2, which is present in both Iso1 and Iso2 (Fig. 5a–d). Iso1 and Iso2 fluorescence, which is composed of the endogenous CNNM2 signal (endogenous Iso1 + Iso2; Fig. 5a, c) and of overexpressed Iso1 (Fig. 5b) or Iso2 (Fig. 5d) signals, is almost identical for both Iso, which are evenly distributed throughout the cells. However, when overexpressed, both Iso1 and Iso2 also seem to be targeted into the nucleus (Fig. 5b, d; Z-stack). This is not the case in −tet cells. The latter might also explain the observation of Wang et al. [45] who have detected CNNM2 as a nuclear protein (see above). Lastly, we immunodecorated C-terminally Strep-tagged Iso1 and Iso2 in transiently transfected HEK293 cells (Fig. 6a and Fig. 7a). Both Iso1-Strep and Iso2-Strep were localized in the periplasmic space and plasmalemma. We have also performed the coimmunolocalization of Iso1-Strep and Iso2-Strep with the mitochondrial marker COXIV (Fig. 6d and Fig. 7d) and for Iso1-Strep also with a MitoTracker (Supplemental Movie 1). Our data indicate that neither of the two Iso is an exclusively mitochondrial protein. Taken together, our data suggest that Iso1 and Iso2 are localized in membranous structures primarily in the periplasmic space of the cell. However, these data also call for careful interpretation of the localization of CNNM2 (its isomorphs) as it is clearly dependent on expression status and probably also on other factors such as Ab specificity.

Mouse and human Iso1 have been shown to transport $Mg^{2+}$ when expressed in genetically distant *Salmonella sp.*- or *Xenopus sp.*-derived expression systems [10, 31, 40]. In contrast, the ability to transport $Mg^{2+}$ has not been confirmed in a homologous expression system (HEK293 cells) and, instead, Stuiver et al. have reported that CNNM2 mediates $Mg^{2+}$-sensitive $Na^+$ currents [41]. Our patch clamp data (Fig. 8) clearly show that, unlike TRPM7 [14, 24, 26], neither of the two tested CNNM2 Iso generates $Na^+$ or $Mg^{2+}$ currents under $Mg^{2+}$ influx-favoring conditions, despite their overexpression. In previously performed studies, the possible "$Mg^{2+}$-sensor" function of CNNM2 was assumed in kidney; however, the possibility that CNNM2 transports $Mg^{2+}$ in an electroneutral mode has not been explicitly excluded [7, 41]. Therefore, we have performed mag-fura 2-assisted $Mg^{2+}$ influx and efflux measurements aimed at identifying the ability of Iso1 and Iso2 to transport $Mg^{2+}$ in an electroneutral mode in transgenic HEK293 cells. Our results have revealed that the overexpression of Iso1 or Iso2 does not lead to an increased $Mg^{2+}$ influx or $Mg^{2+}$ efflux capacity of these cells, when compared with control cells. This is in agreement with our further observation that the total cellular Mg content does not change in dependence on the expression of Iso1 or Iso2 at varying $[Mg^{2+}]_e$ (Fig. 9). Surprisingly, the endogenous $Mg^{2+}$ transport systems (e.g., TRPM7) does not support $Mg^{2+}$ influx at higher $[Mg^{2+}]_e$ resulting in an increased $[Mg]_t$ in −tet and +tet Iso1 and Iso2 cells; however, we have previously reported a similar observation for transgenic HEK293 cells with inducible overexpression of the $Na^+/Mg^{2+}$ exchanger (NME) SLC41A1 [17]. In those cells, $[Mg]_t$ was increased at elevated $[Mg^{2+}]_e$ only when SLC41A1 was overexpressed [17]. Although SLC41A1 is primarily a cellular $Mg^{2+}$ efflux system, at high $[Mg^{2+}]_e$, it works in the reverse mode supporting $Mg^{2+}$ influx (Supplemental Fig. 1), thus feasibly explaining the observed increase of $[Mg]_t$ [17, 18].

A concern might arise as to whether transgenic Iso1 and Iso2 cells possess factors necessary for the proper function of Iso1 and Iso2 in these cells. The transcript of *CNNM2* and also the transcripts of other *MRGs* (*SLC41A1*, *SLC41A2*, *SLC41A3*, *NIPA1*, *MagT1*, *TRPM7*, and *N33*) are detectable in wild-type (wt) HEK293 cells (Supplemental Fig. 4). This indicates that wt HEK293 cells (and also HEK293-derived transgenic cell lines) possess all the major components of the intracellular $Mg^{2+}$ homeostatic network, further implying the presence of all adjacent molecular mechanisms involved in their regulation.

Taken together, these data strongly indicate that neither of the two tested CNNM2 Iso is a bona fide $Mg^{2+}$ transporter in mammalian expression systems.

Subsequently, we examined the complex-forming ability of both Iso1 and Iso2 by performing blue native electroseparation of Iso1 and Iso2 complexes. Both Iso1 and Iso2 seem to form similar, stable protein complexes (C1, C2, C3, C4.1, C4.2, and C5; Fig. 10a, b). However, none of them corresponds size-wise with the complex between Iso1 and Iso2 (dimer, approximately 200 kDa) observed by de Baaij et al. in COS-7 cells with both Iso being co-overexpressed [7]. Coexpression imposes an increased risk of identifying "a false-positive" interaction between the two Iso (both cloned under the very strong promoter, CMV/*p*cDNA3) that otherwise would not occur in unmanipulated cells [7, 32]. Although both Iso1 and Iso2 possess CBS-dimerization domains [40], their ability to form heterodimers and/or homodimers has to be further examined under more physiological conditions.

To identify the spectrum of the potential interactors of Iso1 and Iso2, we performed SU-YTHa. Interestingly, the spectrum of interactors for Iso1 was ten times smaller than that for Iso2. Moreover, the cellular distribution and the functional involvement of Iso2 interactors seemed to be markedly broader than those of Iso1 (Fig. 11a, b). This suggests that Iso2 has a higher potency to form transient protein complexes than Iso1, but that they are not stable enough to be resolved by blue native electroseparation, thus, further indicating that each Iso has a specific non-overlapping role in cellular physiology.

Among the interesting potential interactors of CNNM2, we have identified PARK7/DJ-1 (interactor of Iso1), PINK1, and AMBRA1 (both interactors of Iso2). All three play an important role in the maintenance of mitochondrial homeostasis and the protection against cell death [3, 30]. Billia and colleagues have provided evidence that PARK7/DJ-1 is a unique and nonredundant antioxidant that functions independently of other antioxidative pathways [3]. Moreover, PARK7/DJ-1 has been shown to regulate positively the transcriptional activity of the androgen receptor (AR) [42]. Interestingly, AR is expected to play an important role in the regulation of SLC41A1 [21, 33]. Therefore, we can assume that PARK7/DJ-1 is involved in the regulation of the expression of the $Na^+/Mg^{2+}$ exchanger SLC41A1 and, based on this, in the regulation of IMH [21, 33]. Thus, if CNNM2 plays a role in intracellular and/or extracellular $Mg^{2+}$ sensing, one can further speculate that the interaction with PARK7/DJ-1 initiates the activation of AR, followed by the androgen-responsive element (*ARE*)-mediated activation of the expression of SLC41A1 and the increased $Mg^{2+}$ efflux capacity of the cells. This hypothesis, however, requires testing in forthcoming studies, since little is known about the molecular background that accompanies changes in IMH.

PINK1 has been identified as a key component in the machinery of mitophagy initiation, a process absolutely crucial for the cellular clearance of damaged mitochondria and for healthy mitochondrial homeostasis. Again, on the assumption that CNNM2 is involved in $Mg^{2+}$ sensing, the logic behind a possible CNNM2 (Iso2)-PINK1 interaction could be an up-regulation of mitophagy upon the detection of a $Mg^{2+}$ leak from damaged mitochondria. Although this statement remains hypothetical at present, the interaction between Iso2 and

PINK1 should be studied further, since the multifactorial homeostatic factor CNNM2 seems to be important not only for the regulation of IMH but also for mitochondrial homeostasis.

AMBRA1 is recruited in a Parkin-dependent manner to perinuclear clusters of depolarized mitochondria where it activates PI3K and contributes to their selective autophagic clearance [44]. The intronic variant of AMBRA1 (rs11819869) has been shown to be schizophrenia-related [13]. Interestingly, the CNNM2 variant (rs7914558) has also been revealed to be related to schizophrenia [34]. We hypothesize that the newly discovered putative interaction between AMBRA1 and Iso2 of CNNM2 is highly probable, since variants of both proteins are related to the same disease. Moreover, the involvement of both proteins in the pathology of schizophrenia further substantiates a potential involvement of CNNM2 in the process of mitophagy.

Another link between CNNM2 and PD exists via α-synuclein, a protein associated with an autosomal dominant pattern of PD inheritance. α-synuclein has been shown to modulate neurite outgrowth by interacting with SPTBN1 [22]. SPTBN1 has also been identified as being an integral component of β-amyloid plaques in AD [39]. Here, we have confirmed the interaction of SPTBN1 with both Iso1 and Iso2 by two independent SU-YTHa. We therefore propose that Iso1 and Iso2 are either stabilized by SPTBN1 in cellular membranes or that, particularly in neurons, they play the role of $Mg^{2+}$ sensors in synaptic termini where they contribute to the regulation of vesicular transport [6]. In this regard, a particularly interesting investigation would be to test whether CNNM2 can regulate putative $Mg^{2+}$ transporters HIP14 and HIP14L (from Huntingtin interacting protein 14 and HIP14-like), which have both been implicated in cellular vesicle trafficking [8, 11, 31].

In summary, we conclude that *CNNM2* is a magnesiotropic gene encoding a cellular $Mg^{2+}$ homeostatic factor integral to membranous structures in the periplasmic space and to the plasmalemma. The cellular distribution of CNNM2 and its isomorphs seems however to be markedly dependent on their expression levels. As, to date, all confirmed components of IMH have been shown to be $Mg^{2+}$ transporters per se, CNNM2 therefore seems to be the first factor of IMH having a purely regulatory and not a $Mg^{2+}$ transport function. Both Iso1 and Iso2 form protein complexes of a higher molecular order with an as yet unknown composition. Spectra of identified putative interactors of CNNM2 (in particular of Iso2) suggest that CNNM2 is a principal molecular factor linking IMH with other key mechanisms in the cell, e.g., oxidative stress and mitophagy (mitochondrial homeostasis). The identities of the potential interactors of Iso1 and Iso2 also indicate that CNNM2 plays an important role in the pathophysiology of degenerative diseases. The proposed interactions between the isomorphs of CNNM2 and their putative interactors should be further studied because of their potential clinical importance. The functional difference between Iso1 and Iso2 should also be further examined, as our data indicate that each has a distinctive function in the physiology of the cell.

**Acknowledgments** Our gratitude is due to Martin Marak (Freie Universität Berlin) for competent technical support of the project, to Dr. Svenja Plöger-Meissner (Freie Universität Berlin) for help with the confocal microscopy, to Dr. Mandana Rezwan (Dualsystems Biotech AG) for cooperation with the construction of the cell lines, and to Dr. Katrin Rutschmann (Dualsystems Biotech AG) for cooperation with the SU-YTHa. Our thanks are also extended to Dr. Theresa Jones for linguistic corrections.

This work was supported by research grants from the German Research Foundation (DFG), KO-3586/3-1 and KO-3586/3-2 to MK and by research grant from Protina Pharmazeutische GmbH to JV and MK.

**Contributions** MK designed the study; GS, LMa, KK, LMe, ZZ, NA, AS, KW, AF, RP, and MK performed the experiments and analyzed the data; GS, AF, RP, SI, JRA, and JV contributed to the study design; MK wrote the manuscript. All authors read, edited, and approved the manuscript.

**Compliance with ethical standards**

**Competing interests** JV is a scientific consultant of Protina Pharmazeutische GmbH. Other authors have no conflict of interests to disclose.

## References

1. Arjona FJ, de Baaij JHF, Schlingmann KP, Lameris ALL, van Wijk E, Flik G, Regele S, Korenke GC, Neophytou B, Rust S, Reintjes N, Konrad M, Bindels RJ, Hoenderop JG (2014) CNNM2 Mutations Cause Impaired Brain Development and Seizures in Patients with Hypomagnesemia. PLoS Genet 10(4): doi: 10.1371/journal.pgen.1004267
2. Barbagallo M, Belvedere M, Dominguez LJ (2008) Magnesium homeostasis and aging. Magnes Res 22:235–46. doi:10.1684/mrh.2009.0187
3. Billia F, Hauck L, Grothe D, Konecny F, Rao V, Kim RH, Mak TW (2013) Parkinson-susceptibility gene DJ-1/PARK7 protects the murine heart from oxidative damage in vivo. Proc Natl Acad Sci U S A 110:6085–90. doi:10.1073/pnas.1303444110
4. Bricker DK, Taylor EB, Schell JC, Orsak T, Boutron A, Chen YC, Cox JE, Cardon CM, Van Vranken JG, Dephoure N, Redin C, Boudina S, Gygi SP, Brivet M, Thummel CS, Rutter J (2012) A mitochondrial pyruvate carrier required for pyruvate uptake in yeast, Drosophila, and humans. Science 337:96–100. doi:10.1126/science.1218099
5. Bustin SA, Benes V, Garson JA, Hellemans J, Huggett J, Kubista M, Mueller R, Nolan T, Pfaffl MW, Shipley GL, Vandesompele J, Wittwer CT (2009) The MIQE guidelines: minimum information for publication of quantitative real-time PCR experiments. Clin Chem 55:611–22. doi:10.1373/clinchem.2008.112797
6. Cooper AA, Gitler AD, Cashikar A, Haynes CM, Hill KJ, Bhullar B, Liu K, Xu K, Strathearn KE, Liu F, Cao S, Caldwell KA, Caldwell GA, Marsischky G, Kolodner RD, Labaer J, Rochet JC, Bonini NM, Lindquist S (2006) Alpha-synuclein blocks ER-Golgi traffic and Rab1 rescues neuron loss in Parkinson's models. Science 313:324–8
7. de Baaij JH, Stuiver M, Meij IC, Lainez S, Kopplin K, Venselaar H, Müller D, Bindels RJ, Hoenderop JG (2012) Membrane topology

and intracellular processing of cyclin M2 (CNNM2). J Biol Chem 287:13644–55. doi:10.1074/jbc.M112.342204
8. del Toro D, Alberch J, Lázaro-Diéguez F, Martín-Ibáñez R, Xifró X, Egea G, Canals JM (2009) Mutant Huntingtin impairs post-golgi trafficking to lysosomes by delocalizing optineurin Rab8 complex from the golgi apparatus. Mol Biol Cell 20:1478–92. doi:10.1091/mbc.E08-07-0726
9. Fleig A, Schweigel-Röntgen M, Kolisek M (2013) Solute Carrier Family SLC41, what do we really know about it? Wiley Interdiscip Rev Membr Transp Signal 2(6). doi: 10.1002/wmts.95
10. Goytain A, Quamme GA (2005) Functional characterization of ACDP2 (ancient conserved domain protein), a divalent metal transporter. Physiol Genomics 22:82–9
11. Goytain A, Hines RM, Quamme GA (2008) Huntingtin-interacting proteins, HIP14 and HIP14L, mediate dual functions, palmitoyl acyltransferase and $Mg^{2+}$ transport. J Biol Chem 283:33365–74. doi:10.1074/jbc.M801469200
12. Hahn FM, Xuan JW, Chambers AF, Poulter CD (1996) Human isopentenyl diphosphate: dimethylallyl diphosphate isomerase: overproduction, purification, and characterization. Arch Biochem Biophys 332:30–4
13. Heinrich A, Nees F, Lourdusamy A et al (2013) From gene to brain to behavior: schizophrenia-associated variation in AMBRA1 alters impulsivity-related traits. Eur J Neurosci 38:2941–5. doi:10.1111/ejn.12201
14. Hermosura MC, Monteilh-Zoller MK, Scharenberg AM, Penner R, Fleig A (2002) Dissociation of the store-operated calcium current I(CRAC) and the Mg-nucleotide-regulated metal ion current MagNuM. J Physiol 539:445–58
15. Iotti S, Malucelli E (2008) *In vivo* assessment of $Mg^{2+}$ in human brain and skeletal muscle by $^{31}$P-MRS. Magnes Res 21:157–62
16. Kolisek M, Zsurka G, Samaj J, Weghuber J, Schweyen RJ, Schweigel M (2003) Mrs2p is an essential component of the major electrophoretic $Mg^{2+}$ influx system in mitochondria. EMBO J 22:1235–44
17. Kolisek M, Launay P, Beck A, Sponder G, Serafini N, Brenkus M, Froschauer EM, Martens H, Fleig A, Schweigel M (2008) SLC41A1 is a novel mammalian $Mg^{2+}$ carrier. J Biol Chem 283:16235–47. doi:10.1074/jbc.M707276200
18. Kolisek M, Nestler A, Vormann J, Schweigel-Röntgen M (2012) Human gene SLC41A1 encodes for the $Na^+/Mg^{2+}$ exchanger. Am J Physiol Cell Physiol 302:C318–26. doi:10.1152/ajpcell.00289.2011
19. Kolisek M, Galaviz-Hernández C, Vázquez-Alaniz F, Sponder G, Javaid S, Kurth K, Nestler A, Rodríguez-Moran M, Verlohren S, Guerrero-Romero F, Aschenbach JR, Vormann J (2013) SLC41A1 is the only magnesium responsive gene significantly overexpressed in placentas of preeclamptic women. Hypertens Pregnancy 32:378–89. doi:10.3109/10641955.2013.810237
20. Kolisek M, Sponder G, Mastrototaro L, Smorodchenko A, Launay P, Vormann J, Schweigel-Röntgen M (2013) Substitution p.A350V in $Na^+/Mg^{2+}$ exchanger SLC41A1, potentially associated with Parkinson's disease, is a gain-of-function mutation. PLoS One 8(8). doi: 10.1371/journal.pone.0071096
21. Kolisek M, Montezano AC, Sponder G, Anagnostopoulou A, Vormann J, Touyz RM, Aschenbach JR (2015) PARK7/DJ-1 dysregulation by oxidative stress leads to magnesium deficiency: implications in degenerative and chronic diseases. Clin Sci (Lond) 129:1143–50. doi:10.1042/CS20150355
22. Lee HJ, Lee K, Im H (2012) α-Synuclein modulates neurite outgrowth by interacting with SPTBN1. Biochem Biophys Res Commun 424:497–502. doi:10.1016/j.bbrc.2012.06.143
23. Meyer TE, Verwoert GC, Hwang SJ, et al (2010) Genetic Factors for Osteoporosis Consortium; Meta Analysis of Glucose and Insulin Related Traits Consortium. Genome-wide association studies of serum magnesium, potassium, and sodium concentrations identify six Loci influencing serum magnesium levels. PLoS Genet 6(8). doi: 10.1371/journal.pgen.1001045.
24. Monteilh-Zoller MK, Hermosura MC, Nadler MJ, Scharenberg AM, Penner R, Fleig A (2003) TRPM7 provides an ion channel mechanism for cellular entry of trace metal ions. J Gen Physiol 121:49–60
25. Montell C (2003) $Mg^{2+}$ homeostasis: the $Mg^{2+}$nificent TRPM chanzymes. Curr Biol 13:R799–801
26. Nadler MJ, Hermosura MC, Inabe K, Perraud AL, Zhu Q, Stokes AJ, Kurosaki T, Kinet JP, Penner R, Scharenberg AM, Fleig A (2001) LTRPC7 is a Mg.ATP-regulated divalent cation channel required for cell viability. Nature 411:590–5
27. Nestler A, Sponder G, Rutschmann K, Mastrototaro L, Weise C, Vormann J, Schweigel-Röntgen M, Kolisek M (2013) Nature of SLC41A1 complexes: report on the split-ubiquitin yeast two hybrid assay. Magnes Res 26:56–66. doi:10.1684/mrh.2013.0339
28. Nishizawa Y, Morii H, Durlach J (2007) New perspectives in magnesium research (nutrition and health). Springer-Verlag Ltd., London
29. Ohi K, Hashimoto R, Yamamori H, Yasuda Y, Fujimoto M, Umeda-Yano S, Fukunaga M, Watanabe Y, Iwase M, Kazui H, Takeda M (2013) The impact of the genome-wide supported variant in the cyclin M2 gene on gray matter morphology in schizophrenia. Behav Brain Funct 9:40. doi:10.1186/1744-9081-9-40
30. Okatsu K, Oka T, Iguchi M, Imamura K, Kosako H, Tani N, Kimura M, Go E, Koyano F, Funayama M, Shiba-Fukushima K, Sato S, Shimizu H, Fukunaga Y, Taniguchi H, Komatsu M, Hattori N, Mihara K, Tanaka K, Matsuda N (2012) PINK1 autophosphorylation upon membrane potential dissipation is essential for Parkin recruitment to damaged mitochondria. Nat Commun 3:1016. doi:10.1038/ncomms2016
31. Quamme GA (2010) Molecular identification of ancient and modern mammalian magnesium transporters. Am J Physiol Cell Physiol 298:C407–29. doi:10.1152/ajpcell.00124.2009
32. Rao VS, Srinivas K, Sujini GN, Sunand Kumar GN (2014) Protein-protein interaction detection: methods and analysis. Int J Proteomics 2014:147648. doi:10.1155/2014/147648
33. Romanuik TL, Wang G, Holt RA, Jones SJ, Marra MA, Sadar MD (2009) Identification of novel androgen-responsive genes by sequencing of LongSAGE libraries. BMC Genomics 10:476. doi:10.1186/1471-2164-10-476
34. Rose EJ, Hargreaves A, Morris D, Fahey C, Tropea D, Cummings E, Caltagirone E, Bossu P, Chiapponi C, Piras F, Spalletta G, Gill M, Corvin A, Donohoe G (2014) Effects of a novel schizophrenia risk variant rs7914558 at CNNM2 on brain structure and attributional style. Br J Psychiatry 204:115–21. doi:10.1192/bjp.bp.113.131359
35. Sargenti A, Farruggia G, Malucelli E, Cappadone C, Merolle L, Marraccini C, Andreani G, Prodi L, Zaccheroni N, Sgarzi M, Trombini C, Lombardo M, Iotti S (2014) A novel fluorescent chemosensor allows the assessment of intracellular total magnesium in small samples. Analyst 139:1201–7. doi:10.1039/c3an01737k
36. Schägger H, von Jagow G (1991) Blue native electrophoresis for isolation of membrane protein complexes in enzymatically active form. Anal Biochem 199:223–31
37. Schefe JH, Lehmann KE, Buschmann IR, Unger T, Funke-Kaiser H (2006) Quantitative real-time RT-PCR data analysis: current concepts and the novel "gene expression's CT difference" formula. J Mol Med (Berl) 84:901–10
38. Schmitz C, Perraud AL, Johnson CO, Inabe K, Smith MK, Penner R, Kurosaki T, Fleig A, Scharenberg AM (2003) Regulation of vertebrate cellular $Mg^{2+}$ homeostasis by TRPM7. Cell 114:191–200
39. Sihag RK, Cataldo AM (1996) Brain beta-spectrin is a component of senile plaques in Alzheimer's disease. Brain Res 743:249–57
40. Sponder G, Svidova S, Schweigel M, Vormann J, Kolisek M (2010) Splice-variant 1 of the ancient domain protein 2 (ACDP2)

complements the magnesium-deficient growth phenotype of *Salmonella enterica* sv. *typhimurium* strain MM281. Magnes Res 23:105–14. doi:10.1684/mrh.2010.0206

41. Stuiver M, Lainez S, Will C, Terryn S, Günzel D, Debaix H, Sommer K, Kopplin K, Thumfart J, Kampik NB, Querfeld U, Willnow TE, Nemec V, Wagner CA, Hoenderop JG, Devuyst O, Knoers NV, Bindels RJ, Meij IC, Müller D (2011) CNNM2, encoding a basolateral protein required for renal $Mg^{2+}$ handling, is mutated in dominant hypomagnesemia. Am J Hum Genet 88: 333–43. doi:10.1016/j.ajhg.2011.02.005
42. Takahashi K, Taira T, Niki T, Seino C, Iguchi-Ariga SM, Ariga H (2001) DJ-1 positively regulates the androgen receptor by impairing the binding of PIASx alpha to the receptor. J Biol Chem 276: 37556–63
43. Takeuchi F, Isono M, Katsuya T, Yamamoto K, Yokota M, Sugiyama T, Nabika T, Fujioka A, Ohnaka K, Asano H, Yamori Y, Yamaguchi S, Kobayashi S, Takayanagi R, Ogihara T, Kato N (2010) Blood pressure and hypertension are associated with 7 loci in the Japanese population. Circulation 121:2302–9. doi:10.1161/CIRCULATIONAHA.109.904664
44. van Humbeeck C, Cornelissen T, Vandenberghe W (2011) Ambra1: a Parkin-binding protein involved in mitophagy. Autophagy 7: 1555–6
45. Wang CY, Shi JD, Yang P, Kumar PG, Li QZ, Run QG, Su YC, Scott HS, Kao KJ, She JX (2003) Molecular cloning and characterization of a novel gene family of four ancient conserved domain proteins (ACDP). Gene 306:37–44
46. Wolf FI, Trapani V (2011) MagT1: a highly specific magnesium channel with important roles beyond cellular magnesium homeostasis. Magnes Res 24:S86–91. doi:10.1684/mrh.2011.0288